Journal of Theoretical Biology 424 (2017) 91–109

Contents lists available at ScienceDirect

Journal of Theoretical Biology

journal homepage: www.elsevier.com/locate/jtbi

Regime shifts and ecological catastrophes in a model of plankton-oxygen dynamics under the climate change

Sergei Petrovskii[a,*], Yadigar Sekerci[b], Ezio Venturino[c]

[a] Department of Mathematics, University of Leicester, University Road, Leicester LE1 7RH, U.K
[b] Department of Mathematics, Arts and Science Faculty, Amasya University, 05189 Amasya, Turkey
[c] Dipartimento di Matematica, Università di Torino, via Carlo Alberto 10, 10123 Torino, Italy

ARTICLE INFO

Article history:
Received 26 December 2016
Revised 12 April 2017
Accepted 20 April 2017
Available online 27 April 2017

Keywords:
Phytoplankton
Global warming
Oxygen depletion
Extinction
Early-warning signal
Long-living transient

ABSTRACT

It is estimated that more than a half of the total atmospheric oxygen is produced in the oceans due to the photosynthetic activity of phytoplankton. Any significant decrease in the net oxygen production by phytoplankton is therefore likely to result in the depletion of atmospheric oxygen and in a global mass mortality of animals and humans. In its turn, the rate of oxygen production is known to depend on water temperature and hence can be affected by the global warming. We address this problem theoretically by considering a model of a coupled plankton-oxygen dynamics where the rate of oxygen production slowly changes with time to account for the ocean warming. We show that, when the temperature rises sufficiently high, a regime shift happens: the sustainable oxygen production becomes impossible and the system's dynamics leads to fast oxygen depletion and plankton extinction. We also consider a scenario when, after a certain period of increase, the temperature is set on a new higher yet apparently safe value, i.e. before the oxygen depletion disaster happens. We show that in this case the system dynamics may exhibit a long-term quasi-sustainable dynamics that can still result in an ecological disaster (oxygen depletion and mass extinctions) but only after a considerable period of time. Finally, we discuss the early warning signals of the approaching regime shift resulting in the disaster.

1. Introduction

Global climate change is arguably one of the greatest challenges that the mankind is currently facing (Intergovernmental Panel on Climate Change, 2014). Although its reasons and driving forces (i.e. natural or anthropogenic) remain to be a focus of discussion and some controversy, the basic fact that the average temperature is rising is clearly seen in many observations and can hardly cast any doubt (Hansen et al., 2010; 2006). The effect of the global warming by now remains relatively minor; hence, questions are sometimes asked whether our generation really should bother much about it as the consequences, if any, apparently lie in a remote future. However, a pessimistic scenario of the global warming dynamics predicts the increase in the average Earth's surface temperature by about 4 °C by the end of this century, and this is the threshold where melting of Antarctic ice is expected to start resulting in a flooding on a global scale. It means that the gloomy future is not so remote after all: recently born children have a high chance to experience the full force of awakened Earth during their lifetime.

Global flooding is likely to bring a huge damage to economies and societies all over the world as it will undoubtedly result in poverty, hunger, outbreaks of dangerous diseases etc. However, the overall consequences of the global warming can be far worse than that. Recently, a new ecological disaster resulting from the global warming was reported (Sekerci and Petrovskii, 2015a) that ultimately can kill most of life on Earth. It was shown using a mathematical model of the coupled plankton-oxygen dynamics that, as a response to an increase in average water temperature by several degrees, phytoplankton would stop producing oxygen. As more than one half of the total stock of atmospheric oxygen is produced by the ocean phytoplankton (Harris, 1986; Moss, 2009) (in the process called photosynthesis), such a stop would soon result in the oxygen level dropping down considerably, which could make the air unbreathable for humans and most of animals.

Admittedly, the apocalyptic prediction of the global oxygen depletion remains hypothetical as it was made in a theoretical study based on a rather simple, albeit general, mathematical

* Corresponding author:
E-mail address: sp237@le.ac.uk (S. Petrovskii).

http://dx.doi.org/10.1016/j.jtbi.2017.04.018
0022-5193/

model.[1] More research is required before this could be accepted as a well established scientific fact. A thorough research into this issue should include laboratory studies, microcosm experiments and field studies as well as further development of theory and models. However, a comprehensive empirical study requires considerable resources and careful planning, which may take many years to arrange. On the other hand, the seriousness of the problem, which is literally a "life or death" issue, does not make it sensible to simply wait until relevant field and/or laboratory data become available. Refining and extending the approach based on mathematical modelling is therefore the only way to proceed that is efficient and readily doable. Correspondingly, in this paper we are going to revisit the model of plankton-oxygen dynamics introduced in Sekerci and Petrovskii (2015a) with the purpose to further establish its biological relevance (in particular, by revealing its relation to a class of more realistic models of marine ecosystem) and to check the robustness of the model predictions for different scenarios of global warming. With regard to the latter, we are particularly concerned with the following questions:

- whether it may be possible to avert the catastrophe; in particular, perceiving the disaster approaching, whether it may still be possible and not too late to turn the tide and to avoid the global oxygen depletion
- what are the early warning signals, if any, of the approaching tipping point.

The paper is organized as follows. In Section 2, we discuss how a realistic multi-species mathematical model of a marine ecosystem can be reduced to a simpler, generic model that only accounts explicitly for plankton and oxygen. We then focus on the well-mixed case when the model does not contain space and hence consists of ordinary differential equations. In Section 3, we present the results of the steady states analysis and provide an overview of the bifurcation structure of the system. Scenarios of the global climate change are briefly discussed in Section 4. The corresponding response of the well-mixed system to an increase in the water temperature is then studied by means of numerical simulations in Section 4 where we show that the system collapses when the temperature increases too much. In Section 5, we extend our analysis onto the spatially explicit case and focus on the effect of self-organized pattern formation and how they evolve as a response to the water temperature increase. In Section 6, we will show that the dynamics of the spatial system may exhibit a long-term "quasi-sustainable" dynamics that can still result in an ecological disaster (oxygen depletion and mass extinctions) but only after a considerable period of time. Early warning signals that are observed in the system's dynamics when it approaches the tipping point are discussed too. Finally, we discuss and summarize our results in Section 7.

2. Model equations

Mathematical models of plankton dynamics are numerous (Allegretto et al., 2005; Behrenfeld and Falkowski, 1997; Chapelle, 2000; Denaro, 2013; Fasham, 1978; Fasham et al., 1990; Franke et al., 1999; Huisman and Weissing, 1995; Hull et al., 2000; Kremer and Nixon, 1978; Malchow et al., 2003; Medvinsky et al., 2002; Petrovskii and Malchow, 2004; Steel and Lowe-McConnell, 1980; Valenti, 2015; 2016). They differ by the amount of details explicitly taken into account such as the number of species or taxonomic groups, parametrization of coupling between the components (i.e. feedbacks and functional responses), seasonality and/or weather conditions, explicit or implicit space (in particular, to account for the heterogeneity of the marine environment and/or heterogeneity of the species distribution) etc. The amount of details included into the model also depends on the purpose of the study (as well as, sometimes, on the taste and experience of the authors) and the models available from the literature range from very simple "conceptual" ones to very complicated "realistic" ones.

In a generic dynamical systems' perspective, many marine ecosystem models can be presented as a system of differential equations:

$$\frac{du_i(t)}{dt} = f_i(u_1, \ldots, u_n, t), \qquad i = 1, \ldots, n, \tag{1}$$

where n is the total number of components explicitly included into the model, i.e. species or groups (plankton, bacteria etc.) and substances (e.g. nutrients), u_i is the concentration or density of the ith component at time t, and function f_i is the species growth rate that takes into account intra- and interspecific interactions such as competition, grazing etc. Note that model (1) does not contain space as it corresponds to a "well-mixed" system where all components are distributed uniformly over the space (e.g. over the top layer of the ocean). In case the assumption of spatial homogeneity is irrelevant, the model should be extended to include explicit space and the corresponding fluxes (e.g. due to turbulent transport); we will consider this case in more detail in Section 5.

As an instructive example and the starting point for our analysis, we consider the well-known model of plankton dynamics developed by Fasham et al. (1990); see Fig. 1. Apparently, in this case $n = 7$, so that system (1) consists of seven equations. This is a model of intermediate complexity that is relatively easy to implement on a computer. In this paper, however, our goal is to make an insight into some generic properties of the plankton dynamics, and for this purpose model (1) with $n = 7$ is excessively complex and contains too many specific details. Indeed, understanding of the system properties is greatly facilitated by a possibility of an analytical study (such as, for instance, the existence and stability of steady states) but this is hardly possible in a model consisting of seven nonlinear ODEs. We therefore look for some possible simplification and generalization of the Fasham model keeping our main focus on phyto-zooplankton dynamics.

We first assume that nitrate and ammonium can be combined to a single component, i.e. nutrients that are needed for phytoplankton growth. We then notice that, in the course of time, detritus decays through a chain of biochemical reactions to the dissolved organic matter (DOM) which consists of organic molecules of various kinds that includes nitrogen, carbon and other elements as their building blocks. A part of DOM can be re-used as nutrients by the phytoplankton, sometimes straightforwardly, in other cases after its utilization by bacteria (Fasham et al., 1990). Bacteria hence play an important role in the remineralization cycle in the ocean and can, under some conditions, become a bottleneck that slows down the phytoplankton growth (Banse, 1995). In accordance with our intention to keep the model as simple as possible, we assume that the concentration of bacteria in the ocean water is always maintained at some stable intermediate level not to impede the phytoplankton growth[2], and nutrients are always available in a sufficient amount not to limit the phytoplankton growth either. Note that the latter assumption is also justified by the fact that the deep ocean is known to be a huge reserve of nutrients that are transported to the upper, productive layer by water flows due to turbulent exchange and upwellings (Mann and Lazier, 1996).

[1] Moreover, the pessimistic scenario of the global warming by 4 °C mentioned above is by itself the worst case scenario and thus is not very probable. A majority of predictions give a much softer estimate of the expected temperature increase of about 2 °C.

[2] Note that for the purposes of this study cyanobacteria (also known as blue-green algae) are included into phytoplankton, because they play a similar role in the oxygen production through photosynthesis.

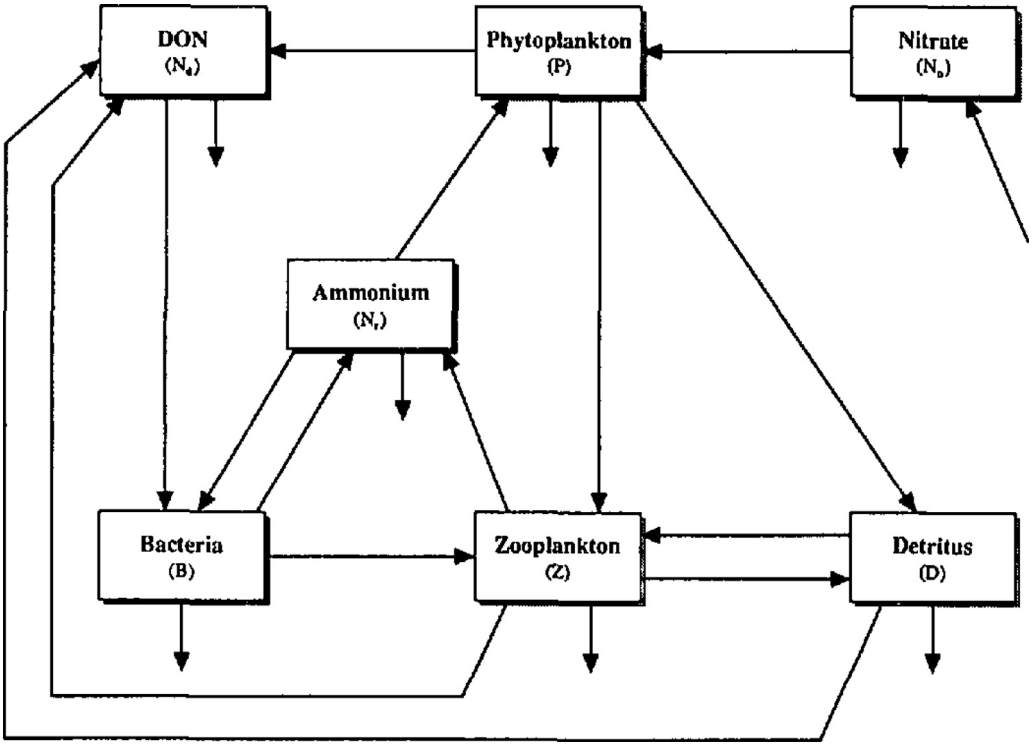

Fig. 1. Flowchart of the nitrogen-based Fasham model of plankton dynamics (Fasham et al., 1990). Arrows show the direction of the matter flow.

We now note that one important component missing from the original Fasham model is the dissolved oxygen. Oxygen is produced by phytoplankton in the upper (photic) layer of the ocean and is consumed by all marine species through breathing; see Fig. 2. Oxygen is also needed for many biochemical reactions (including those involved in the remineralization cycle) that constantly go on in the ocean water. The level of dissolved oxygen is regarded as an important indicator of the marine ecosystem health (Breitburg et al., 1997). On top of the oxygen that is consumed within the marine ecosystem, eventually a considerable part of the produced oxygen is transported through the ocean-air interface to contribute to the atmospheric oxygen. It is estimated that more than one half of atmospheric oxygen is produced in the ocean (Harris, 1986).

The above simplifications effectively reduces the Fasham model to a simple two-component phyto-zooplankton system which we now extend by including the dissolved oxygen; see Fig. 2. We therefore arrive at the following conceptual three-component model of the coupled plankton-oxygen dynamics which we write in the following form:

$$\frac{dc}{dt} = Af(c)u - u_r(c,u) - v_r(c,v) - mc, \tag{2}$$

$$\frac{du}{dt} = g(c,u) - e(u,v) - \sigma u, \tag{3}$$

$$\frac{dv}{dt} = \kappa(c)e(u,v) - \mu v, \tag{4}$$

where c is the concentration of oxygen, u and v are, respectively, the densities of phytoplankton and zooplankton at time t. Here $Af(c)$ describes the rate of oxygen production per unit phytoplankton mass due to photosynthesis. Whilst function $f(c)$ describes the rate of increase in the concentration of the dissolved oxygen because of its transport from phytoplankton cells to the surrounding water, factor A takes into account the effect of the environmental factors (such as the water temperature) on the rate of oxygen production inside the cells. Function $g(c, u)$ describes the phytoplankton growth rate which is known to be correlated to the rate of photosynthesis (Franke et al., 1999); we therefore assume it to depend on the amount of available oxygen. Indeed, as all living beings, phytoplankton needs oxygen for its metabolism, hence some dependence of the phytoplankton growth rate on the oxygen concentration is feasible, at least under anoxic conditions. Terms u_r and v_r in Eq. (2) are the rates of oxygen consumption by phytoplankton and zooplankton, respectively, because of their respiration. The coefficient m is the rate of oxygen loss due to the natural depletion (e.g. due to biochemical reactions in the water). The term e in Eq. (3) describes feeding of zooplankton on phytoplankton. The consumed phytoplankton biomass is transformed into the zooplankton biomass with efficiency κ, see the first term in the right-hand side of Eq. (4). Since the well-being of zooplankton obviously depends on the oxygen concentration (so that, ultimately, it dies if there is not enough oxygen to breathe), we assume that $\kappa = \kappa(c)$. Coefficients σ and μ are the natural mortality rates of the phyto- and zooplankton, respectively.

We mention here that, whilst in the above a realistic model has been reduced to a simpler three-component model (2)–(4) based on a heuristic argument, it appears possible to establish the role of the conceptual model (2)–(4) more rigorously. Namely, using the mathematical techniques known as the comparison principle (or comparison theorem), one can prove that model (2)–(4) gives an upper bound for a food web type class of more complicated (and more realistic) models; see Appendix for details.

It is not possible to deal with system (2)–(4) until all the feedbacks are specified. Based on a biologically meaningful argument as well as some evidence from field observation, see Sekerci and Petrovskii (2015a; 2015b) for details, system (2)–(4) takes the following more specific form:

$$\frac{dc}{dt} = \frac{Ac_0u}{c+c_0} - \frac{\delta uc}{c+c_2} - \frac{\nu cv}{c+c_3} - mc, \tag{5}$$

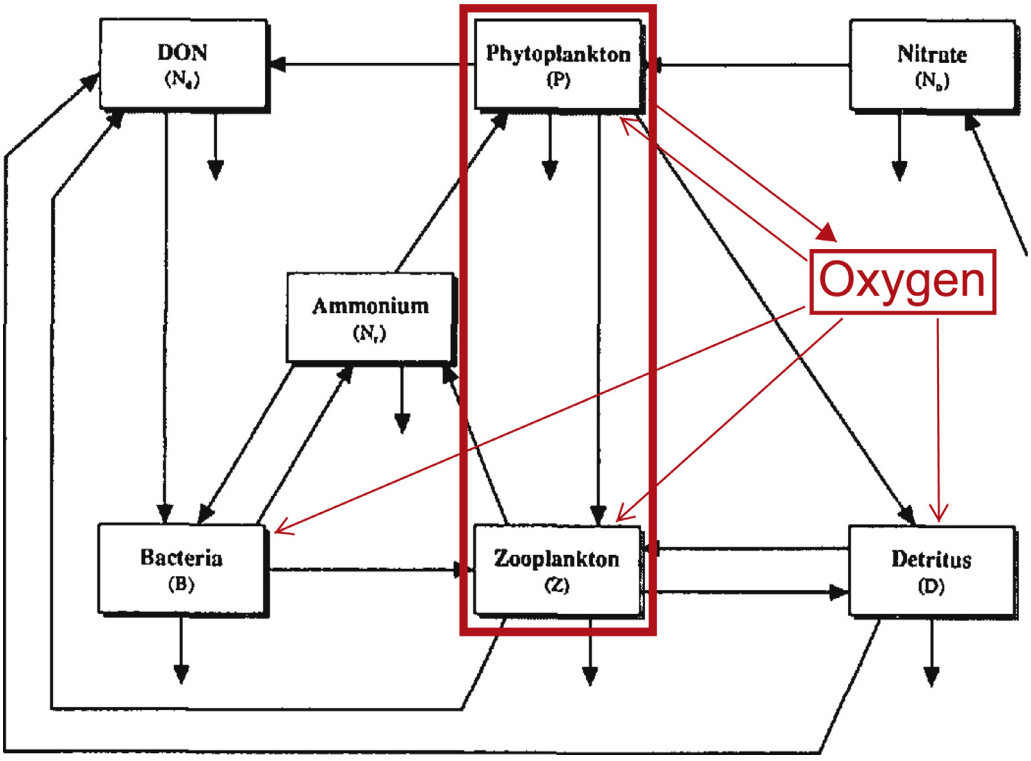

Fig. 2. Reduced Fasham model with the main focus kept on phyto-zooplankton (inside of the red rectangle) and extended to include oxygen. Red arrows show the oxygen flow between different components of the marine ecosystem; see details in the text.(For interpretation of the references to colour in this figure legend, the reader is referred to the web version of this article.)

$$\frac{du}{dt} = \left(\frac{Bc}{c+c_1} - \gamma u\right)u - \frac{\beta uv}{u+h} - \sigma u, \tag{6}$$

$$\frac{dv}{dt} = \frac{\eta c^2}{c^2+c_4{}^2}\,\frac{\beta uv}{u+h} - \mu v. \tag{7}$$

Here $c_0, \ldots, c_4$ are the half saturation constants of the Monod-type kinetics of the corresponding processes, δ and ν are parameters quantifying the rate of oxygen consumption due to, respectively, phyto- and zooplankton respiration, B is the linear per captita phytoplankton growth rate (under non-anoxic conditions, i.e. where oxygen is not a limiting factor), β quantifies the rate of zooplankton grazing on phytoplankton, h being the half-saturation density, γ describes a density-dependent decrease in the phytoplankton growth (e.g. due to intra-specific competition or self-shading), σ and μ are the mortality rates of phyto- and zooplankton, respectively, and η is the maximum feeding efficiency ($0 < \eta < 1$).

Since a considerable part of our study will use numerical simulations, it is convenient to introduce dimensionless variables and parameters. Correspondingly, we consider

$$t' = tm, \qquad c' = \frac{c}{c_0}, \qquad u' = \frac{\gamma u}{m}, \qquad v' = \frac{\beta v}{m} \tag{8}$$

and the new (dimensionless) parameters as

$$\hat{B} = \frac{B}{m}, \quad \hat{A} = \frac{A}{c_0\gamma}, \quad \hat{\delta} = \frac{\delta m}{c_0\gamma}, \quad \hat{\nu} = \frac{\nu m}{\beta c_0}, \quad \hat{\sigma} = \frac{\sigma}{m}, \quad \hat{\mu} = \frac{\mu}{m}, \tag{9}$$

$$\hat{h} = \frac{\gamma h}{m}, \quad \hat{\eta} = \frac{\eta\beta}{m}, \quad \text{and} \quad \hat{c}_i = \frac{c_i}{c_0} \quad \text{where} \quad i = 1, 2, 3, 4. \tag{10}$$

Eqs. (5–7) then take the following form:

$$\frac{dc}{dt} = \frac{Au}{c+1} - \frac{\delta uc}{c+c_2} - \frac{\nu cv}{c+c_3} - c, \tag{11}$$

$$\frac{du}{dt} = \left(\frac{Bc}{c+c_1} - u\right)u - \frac{uv}{u+h} - \sigma u, \tag{12}$$

$$\frac{dv}{dt} = \frac{\eta c^2}{c^2+c_4{}^2}\,\frac{uv}{u+h} - \mu v, \tag{13}$$

where primes and hats are omitted for notation's simplicity.

3. Steady states, bifurcations and dynamics

A convenient first step in revealing the properties of the system (11)–(13) is to consider the existence and stability of its steady states (equilibria). By definition, a steady state is a solution of the following system of algebraic equations:

$$\frac{Au}{c+1} - \frac{\delta uc}{c+c_2} - \frac{\nu cv}{c+c_3} - c = 0, \tag{14}$$

$$\left(\frac{Bc}{c+c_1} - u\right)u - \frac{uv}{u+h} - \sigma u = 0, \tag{15}$$

$$\frac{\eta c^2}{c^2+c_4{}^2}\,\frac{uv}{u+h} - \mu v = 0. \tag{16}$$

It is readily seen that, for any parameter values, there always exists the trivial steady state $E_0 = (0, 0, 0)$ and it is always stable. The latter can be established straightforwardly by calculating the eigenvalues of the corresponding Jacobian as calculations are simple in this case.

Under some restrictions on the parameter values – in particular, A should be sufficiently large, see Sekerci and Petrovskii (2015a) for

details – there exist two boundary steady states where zooplankton is absent, $E_i = (\tilde{c}_i, \tilde{u}_i, 0)$, $i = 1, 2$, that are solutions of the following system:

$$\frac{A\tilde{u}_i}{\tilde{c}_i + 1} - \frac{\delta \tilde{u}_i \tilde{c}_i}{\tilde{c}_i + c_2} - \tilde{c}_i = 0, \tag{17}$$

$$\left(\frac{B\tilde{c}_i}{\tilde{c}_i + c_1} - \tilde{u}_i \right) \tilde{u}_i - \sigma \tilde{u}_i = 0. \tag{18}$$

which is obviously a reduction of system (14)–(16) corresponding to $v = 0$. It is readily seen that other nontrivial reductions of system (14)–(16) such as $c = 0$ or $u = 0$ are not possible; hence there are no other boundary equilibria other than E_1 and E_2.

Regarding the stability of the boundary steady states, one of them (say E_1) is always unstable whilst the other (E_2) can be stable or unstable. Unfortunately, analytical calculation of the eigenvalues is not possible in this case as it would require solving the heavily nonlinear system (14)–(16). (Note that in order to consider stability of the boundary steady states we need to know all three eigenvalues, so that considering the eigenvalues of the reduced system (17) and (18) is not sufficient.) Alternatively, the change in stability of E_2 can be revealed in numerical simulations; see below.

Apart from the trivial and semi-trivial steady states, there can also exist a positive (coexistence) equilibrium $E_3 = (\bar{c}, \bar{u}, \bar{v})$ which is a nontrivial solution of system (14)–(16). It does not seem possible to obtain analytical conditions of its existence and stability because of the complexity of system (14)–(16) and the corresponding Jacobian. Instead, we address this issue by numerical simulations. For a specific parameter set and certain initial conditions, the system (11)–(13) is solved numerically over a sufficiently long time interval. The properties of its large-time dynamics are then analyzed to check what attractor of the system the solution has converged to, e.g. E_0, E_3 or else.

Note that a regular numerical investigation of system (11)–(13) is a challenging task as the system contains twelve parameters. Investigation of its properties in the whole 12-dimensional parameter space is hardly possible. Instead, we choose A, B and c_1 as controlling parameters and then reveal, through intense numerical simulations, the system properties in different domains of the corresponding parameter planes (A, B) and (B, c_1) keeping all other parameters fixed at some hypothetical value. Once the choice of controlling parameters (that will act as well as the bifurcation parameters) is specified, simulations can be done efficiently using a numerical continuation technique, e.g. see Allgower and Georg (2003).

The structure of the plane (A, B) thus revealed in numerical simulations is shown in Fig. 3 (obtained for other parameters fixed as $c_1 = 0.7$, $c_2 = 1$, $c_3 = 1$, $c_4 = 1$, $\nu = 0.01$, $\eta = 0.7$, $\mu = 0.1$, $h = 0.1$, $\sigma = 0.1$ and $\delta = 1$). Outside of the tongue-shaped domain in the (A, B) parameter plane, the trivial E_0 extinction state is the only attractor. Sustainable dynamics of the system is only possible for parameters inside the tongue-shaped domain.

A closer look reveals that, when the parameters vary inside the tongue-shaped domain, the system undergoes a series of bifurcations. Examples of the corresponding system dynamics are shown in Fig. 4 for increasing values of A (fixing $B = 2.5$), so that the corresponding point in the parameter plane goes across the tongue-shaped domain. We readily observe that for a sufficiently small A, i.e. before entering the tongue-shaped domain, in the course of time the system fast converges to E_0; see Fig. 4a. Obviously, it means that the plankton-oxygen system is not sustainable in that parameter range. Once A increases over a certain critical value, a saddle-node bifurcation occurs where the pair of boundary states E_1 and E_2 is born, E_2 being a stable node. Correspondingly, in this parameter range the system converges to the zooplankton-free

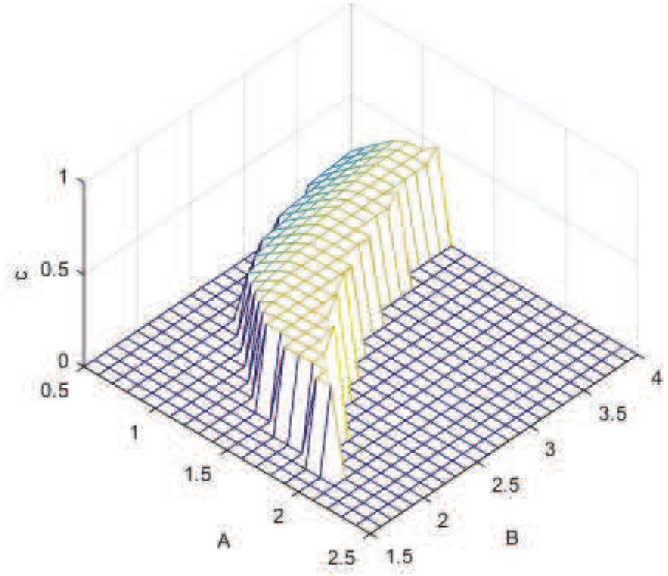

Fig. 3. Structure of the (A, B) parameter plane. The surface shows the maximum value of the oxygen concentration that can be reached in the large-time limit. Correspondingly, sustainable dynamics is only possible inside the tongue-shaped domain, for values of A and B outside of the domain the only attractor is the extinction state E_0. More details are given in the text.

state E_2; see Fig. 4b. With a further increase in A, a transcritical bifurcation happens where the stable node E_3 branches off E_2 and E_2 becomes unstable. In this parameter range, all three components of the system (i.e. oxygen, phyto- and zooplankton) converge to some positive steady state values, see Fig. 4c; hence the system becomes fully sustainable.[3] With a further increase in A, E_3 changes its monotone stability to oscillatory stability (Fig. 4d): the stable node becomes a stable focus. Eventually, for a further increase in A, the focus loses its stability through a Hopf bifurcation and a stable limit cycle emerges; in this parameter range the system dynamics is oscillatory, see Fig. 4e. Finally, for a further increase in A (that takes its value to the other side of the tongue-shaped domain in Fig. 3) the limit cycle disappears in a homoclinic bifurcation, in this parameter range the system is not sustainable any more and the initial conditions eventually converge to the extinction state E_0, typically after a number of oscillations of increasing amplitude.

Putting all the above results together, we conclude that the boundary of the domain in the (A, B) parameter plane where the system is capable of sustainable dynamics is made by two bifurcation curves, i.e. the saddle-node bifurcation curve at lower values of A (the left-hand side of the tongue-shaped domain in Fig. 3) and the homoclinic bifurcation at higher values of A (the right-hand side of the tongue-shaped domain in Fig. 3). We cannot find an analytical description of these curves but they are obtained in simulations.

Numerical simulations of the system (11)–(13) using B and c_1 as the controlling/bifurcation parameters reveals a similar structure in the (B, c_1) plane; see Fig. 5. Sustainable dynamics of the system is only possible within a tongue-shaped domain, outside of the domain extinction is the only option. For the parameters inside the domain, the system undergoes a succession of bifurcations similar to the one described above; we do not show details for sake of brevity.

[3] We recall here that, as the trivial steady state E_0 is always stable, the system exhibits bistability so that there always exists a range of initial values that converge to extinction.

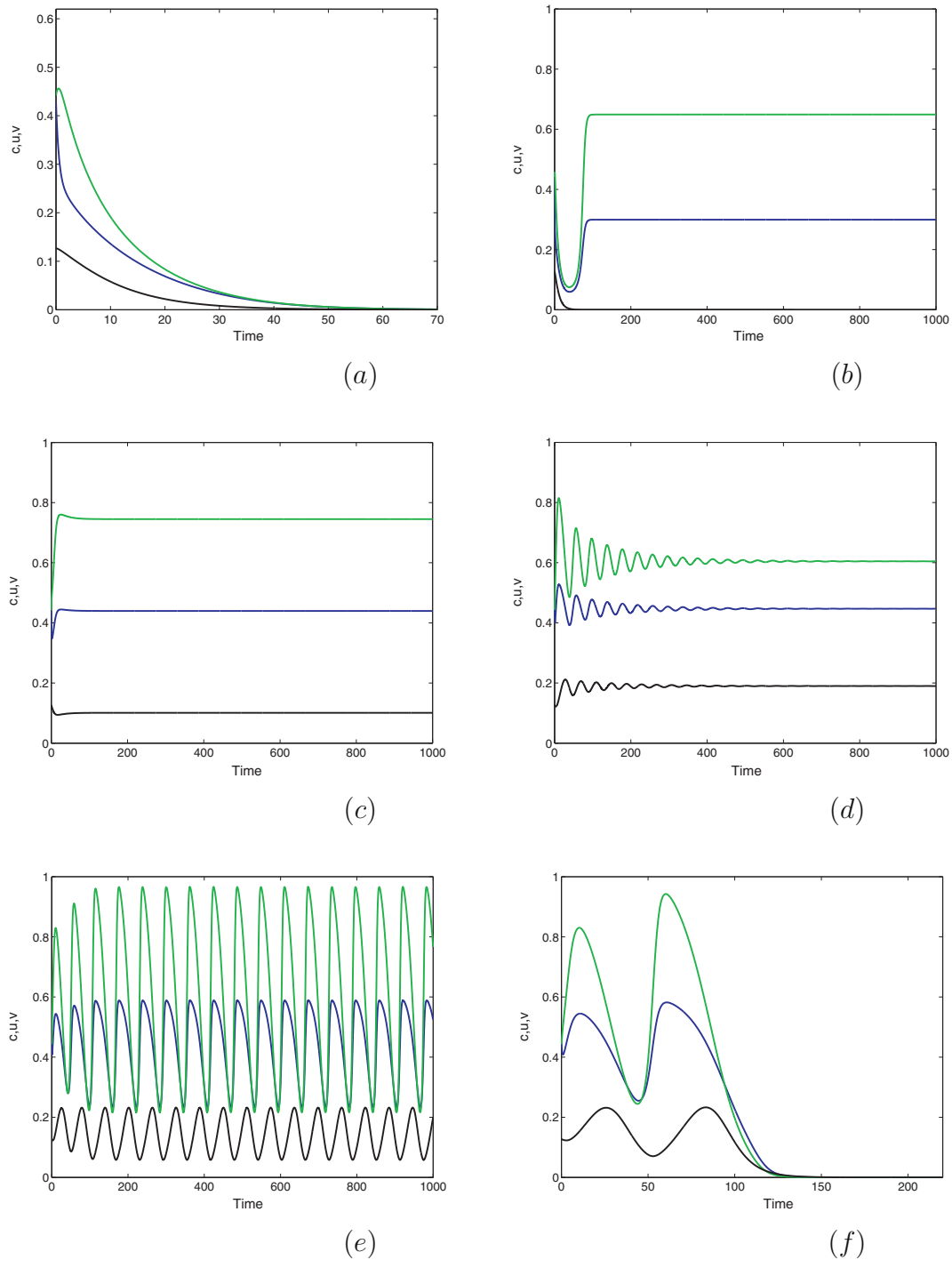

Fig. 4. Change in the system dynamics for $B = 2.5$ and different values of A when the corresponding point in the (A, B) parameter plane moves across the tongue-shaped domain shown in Fig. 3: (a) $A = 0.89$, (b) $A = 0.899$, (c) $A = 1.29$, (d) $A = 1.518$, (e) $A = 1.558$ and (f) $A = 1.56$. Blue, green and black colors are for oxygen, phyto- and zooplankton, respectively. See the main text for more details and other parameter values. (For interpretation of the references to colour in this figure legend, the reader is referred to the web version of this article.)

4. Scenarios of climate change

There is considerable scientific evidence collected over the last two decades showing that the average global temperature has been increasing during the last century, e.g. see Hansen et al. (2010; 2006). On top of a clear trend upwards, the global temperature shows prominent variation between different years or decades, e.g. see Fig. 6. Albeit the tendency to increase is apparent, the dependence of the global temperature on time is complicated, because it arises as an interplay between a variety of deterministic and stochastic factors. A realistic model of the global climate change with an ambition to provide a detailed specific forecast would need to account for the details of temperature dependence. Our goal in this paper is, however, much more modest. We do not claim to provide a quantitative prediction of the future climate change dynamics. Instead, we endeavor to make a *qualitative* insight into a possible effect of the increase in the ocean temperature on the rate of oxygen production by marine phytoplankton.

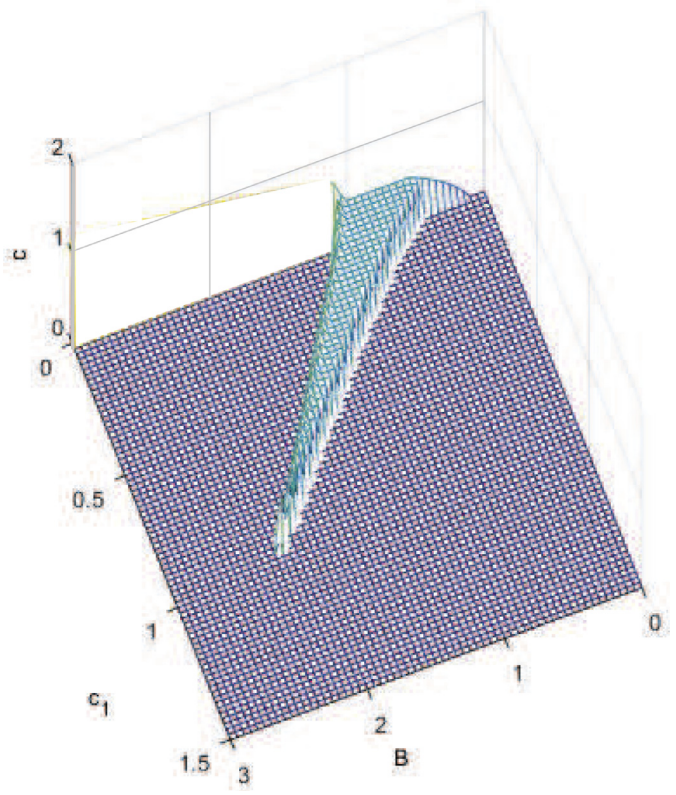

Fig. 5. Structure of the (B, c_1) parameter plane obtained for $A = 2$ and other parameters as in Fig. 3. The surface shows the maximum value of the oxygen concentration reached in the large-time limit. Sustainable dynamics is only possible inside the tongue-shaped domain, for values of B and c_1 outside of the domain the only attractor is the extinction state E_0.

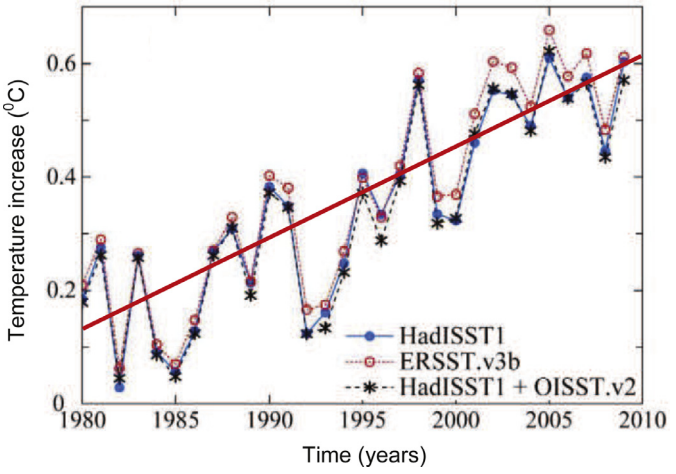

Fig. 6. Global average temperature of the ocean surface against time, adapted from Hansen et al. (2010). Different symbols/colors correspond to data from different sources; see Hansen et al. (2010) for details. The thick red line shows a linear approximation of the trend. (For interpretation of the references to colour in this figure legend, the reader is referred to the web version of this article.)

For this purpose, it is important to take into account the general tendency but not necessarily the details. Correspondingly, to describe the trend one can use a simple function, cf. the thick red line in Fig. 6.

Having decided about the parametrization of the temperature dependence on time, how can we account for it in terms of the model (11)–(13)? The water temperature is known to have various effects on plankton functioning (Andersson et al., 1994; Eppley, 1972). In particular, there is considerable evidence that it can affect the rate of oxygen production (Childress, 1976; Hancke and Glud, 2004; Jones, 1977; Li et al., 1984; Robinson, 2000). In this section, we mostly focus on the case where the temperature affects the oxygen production rate; how the results may change if the temperature effect on other processes is taken into account (e.g. phytoplankton growth rate) will be discussed in Section 7.

A question remains as to whether the oxygen production rate tends to decrease or increase when the water temperature increases. There is certain empirical evidence that the rate tends to go down when the temperature increases; however, it was only observed for a few particular phytoplankton species and under some rather special conditions, cf. (Robinson, 2000). Altogether, available empirical evidence is inconclusive. Correspondingly, we will address both cases of the oxygen production rate being either an increasing or a decreasing function of the temperature.

We now recall that in our model (11)–(13) the rate of the oxygen production is quantified by parameter A. Therefore, in order to take into account the effect of global warming, we now consider A to be a function of time, $A = A(t)$. We begin with the case when the oxygen production rate increases along with the water temperature. Correspondingly, A is an increasing (or, more generally, non-decreasing) function of time. Following the argument above, we consider $A(t)$ to be a simple function to only account for the general trend but not for details.

In our previous work (Sekerci and Petrovskii, 2015a), we considered A to be a linear function of time. Correspondingly, we assumed that the warming would go on indefinitely, i.e. that A should be an (linearly) increasing function of time for any $t > 0$. It was shown in Sekerci and Petrovskii (2015a) that for a sufficiently high increase in the water temperature a regime shift happens, i.e. sustainable oxygen production becomes impossible and the system's dynamics leads to plankton extinction and oxygen depletion (Sekerci and Petrovskii, 2015a). However, the case of an increase in A going on for an indefinitely long time is not entirely realistic. Firstly, it seems plausible that there may be geophysical mechanisms preventing the temperature from increasing too much (or for too long). Secondly, nowadays there seems to be considerable amount of political will to eventually produce a binding global treaty to drastically cut CO_2 production and hence to, hopefully, stop global warming. Correspondingly, in this paper we consider the case when, after a certain period of increase, the temperature is set on a new value. A simple parametrization of this scenario is given by the following function:

$$A(t) = \begin{cases} A_0, & 0 \le t \le t_1, \\ A_0 + \omega(t - t_1), & t_1 < t < t_2, \\ A_1, & t \ge t_2, \end{cases} \tag{19}$$

see Fig. 7. Here $t_2 - t_1 = \tau$ is the duration of the climate change, A_0 is the rate of oxygen production 'before change', A_1 is the rate of oxygen production 'after change' and $\omega = (A_1 - A_0)/\tau$ is the rate of the global warming.

We mention here that, with A being a function of time, the system (11)–(13) is not autonomous and strictly speaking the results of the steady state analysis done in Section 3 do not apply. However, the global warming is a slow process and hence the corresponding rate of increase in A is likely to be very small. In this case, one can expect that the properties of the non-autonomous system are well approximated by the dynamics of the corresponding autonomous system observed for different values of A; see Section 3.

We now perform numerical simulations of the plankton-oxygen system (11)–(13) with A given by (19) in order to reveal possible system's response to different scenarios of climate change, in particular as quantified by different values of parameters A_0,

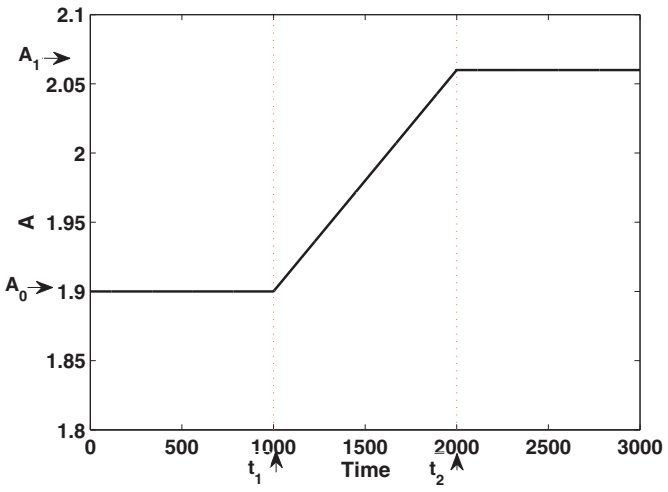

Fig. 7. Sketch of A vs time shown for $A_0 = 1.9$, $A_1 = 2.06$, $t_2 = 2000$ and $t_1 = 1000$.

A_1 and τ. For the initial value A_0 of the oxygen production rate, we assume that the ecosystem was in a safe state. In terms of the system (11)–(13), it means that the coexistence state E_3 is either stable or unstable but surrounded by a stable limit cycle (see Fig. 4c–e), so that the parameters are inside the tongue-shaped domain corresponding to the sustainable dynamics of the system; see Figs. 3 and 5. For the simulations shown below, we fix other parameters at some hypothetical values as $B = 1.8$, $\gamma = 1$, $\sigma = 0.1$, $c_1 = 0.7$, $c_2 = c_3 = c_4 = 1$, $\nu = 0.01$, $\beta = 0.7$, $\mu = 0.1$, $h = 0.1$. For the initial conditions, we use $c_0 = 0.385$, $u_0 = 0.3$ and $v_0 = 0.1$.

Fig. 8 shows the oxygen concentration and plankton densities vs time obtained for $A_0 = 2$, $A_1 = 2.05$, $t_1 = 1000$ and $\tau = 1000$. For this initial value of the oxygen production rate, E_3 is a stable focus but the parameters are close to the Hopf bifurcation. Correspondingly, over the period $0 < t < t_1$ when $A = A_0$, oscillations slowly converge to the steady state values, the amplitude of the oscillations decreasing with time. The increase in A happening for $t_1 < t < t_2$ brings the system beyond the Hopf bifurcation point, so that, once the oxygen production rate stabilizes at the new value $A = A_1$, the dynamics becomes oscillatory. Since A_1 remains inside the parameter range of sustainable dynamics, the oscillations are sustainable and no extinction happen.

However, for a somewhat larger value of A_1, the dynamics becomes different; see Fig. 9. In this case, the gradual increase in A eventually takes the system out of the parameter range of the sustainable dynamics (cf. the tongue-shaped domain in Fig. 3). When t approaches t_2, the system does not possess a stable nontrivial attractor any more (the stable limit cycle disappears in a nonlocal bifurcation), the only attractor being the extinction state. Correspondingly, plankton goes extinct and oxygen is depleting fast. System's dynamics for a larger value of A_1 follows a similar scenario. Fig. 10 shows the simulation results obtained for $A_1 = 2.2$. Since for the fixed value of τ the larger A_1 corresponds to a higher rate of change ω, in this case the catastrophe occurs earlier, well before $A(t)$ reaches its final value A_1.

We therefore conclude that an increase in A over a certain critical value, i.e. an increase that takes the system out the 'safe' parameter domain of sustainable dynamics, results in plankton extinction and oxygen depletion. We mention here that this conclusion is confirmed by numerous simulations performed for other values of parameters A_1 as well as for different values of B and c_1; we do not show them here for sake of brevity.

Compared to that of A_1, the role of the initial value A_0 is different and relatively minor. Fig. 11 shows the results obtained for the same 'supercritical' value $A_1 = 2.2$ but a larger $A_0 = 2.048$. For this value of A_0, prior to the warming the system appears to be beyond the Hopf bifurcation point and hence exhibits stable oscillations. Once A starts increasing, it soon takes the system out of the parameter range of sustainable dynamics, which results in fast plankton extinction and oxygen depletion. Therefore, a larger value of A_0 results in the plankton extinction/oxygen depletion catastrophe happening earlier. The generality of this conclusion can be seen from the following argument. Let A_{cr} be the critical value where the system crosses (in the parameter space) the boundary of the domain of sustainable dynamics and let t_{cr} be the moment when it happens. From Eq. (19), we obtain:

$$t_{cr} = t_1 + \tau \frac{A_{cr} - A_0}{A_1 - A_0}, \tag{20}$$

where $A_1 > A_{cr} > A_0$. It is readily seen that t_{cr} is a monotonously decreasing function of A_0; therefore, for the same duration of

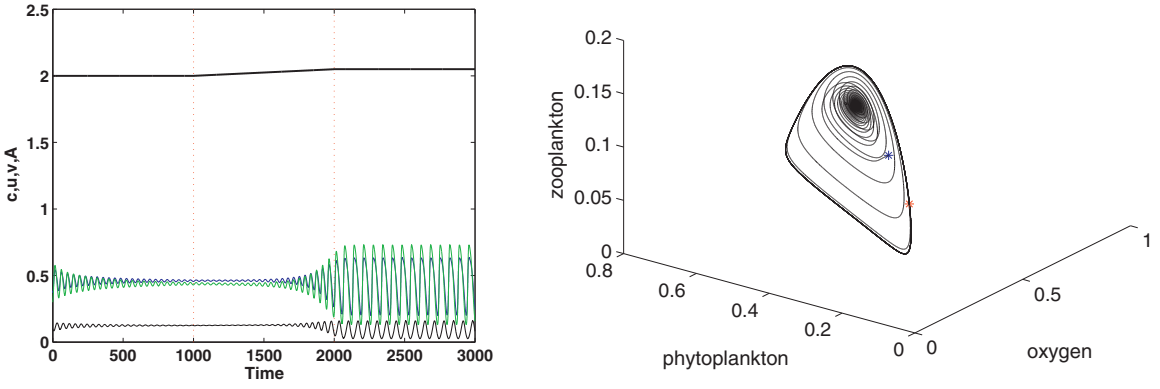

(a) (b)

Fig. 8. (a) Oxygen concentration (blue) and phytoplankton and zooplankton densities (green and black, respectively) against time obtained for $A_0 = 2$, $A_1 = 2.05$, $t_1 = 1000$, $\tau = 1000$. Other parameters are given in the text. The thick black line at the top shows $A(t)$. (b) Corresponding system trajectory in the phase space of the system. The blue star shows the initial conditions, the red star shows the system state at the end of the simulation run. (For interpretation of the references to colour in this figure legend, the reader is referred to the web version of this article.)

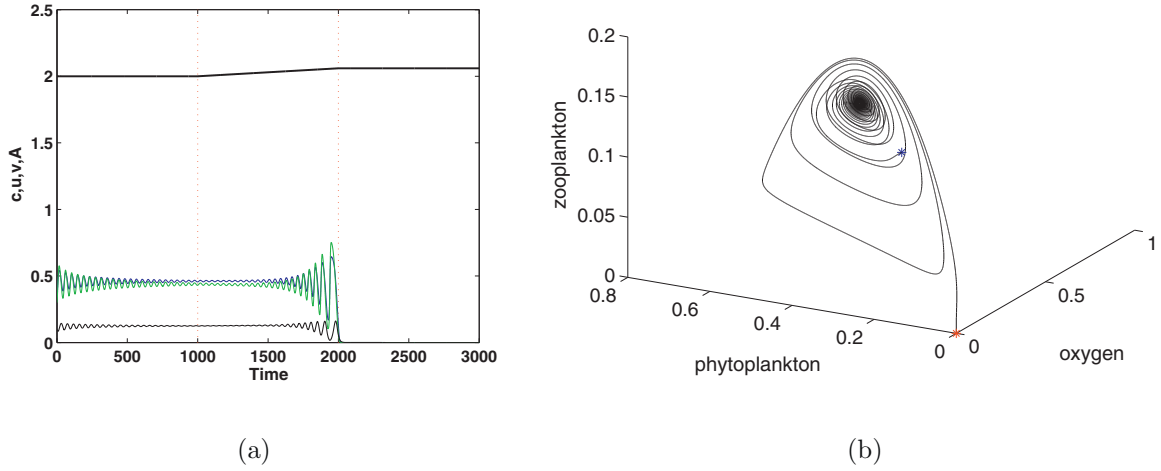

Fig. 9. (a) Oxygen concentration (blue) and phytoplankton and zooplankton densities (green and black, respectively) against time obtained for $A_0 = 2$ and $A_1 = 2.06$. Other parameters are the same as in Fig. 8. The thick black line at the top shows $A(t)$. (b) Corresponding system trajectory in the phase space of the system. The blue star shows the initial conditions, the red star shows the system state at the end of the simulation run. (For interpretation of the references to colour in this figure legend, the reader is referred to the web version of this article.)

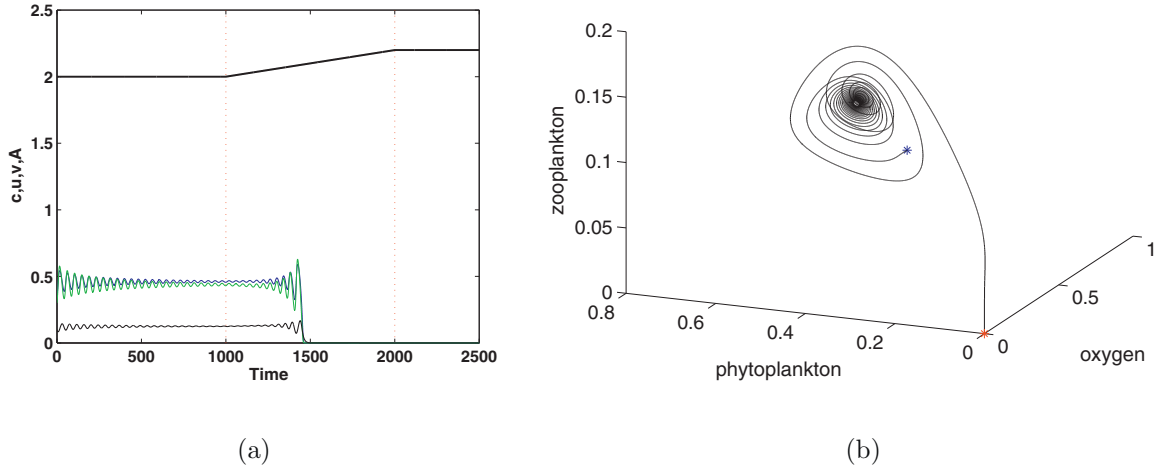

Fig. 10. (a) Oxygen concentration (blue) and phytoplankton and zooplankton densities (green and black, respectively) against time obtained for $A_0 = 2$ and $A_1 = 2.2$. Other parameters and the initial conditions are the same as in Fig. 8. The thick black line at the top shows $A(t)$. (b) Corresponding system trajectory in the phase space of the system. The blue star shows the initial conditions, the red star shows the system state at the end of the simulation run. (For interpretation of the references to colour in this figure legend, the reader is referred to the web version of this article.)

change τ and the final value A_1, larger values of A_0 correspond to smaller values of t_{cr}.

5. Spatial system

The above analysis was done for a nonspatial system when all the densities are distributed uniformly over space. Although this approximation of a "well mixed" system is frequently used in the literature (Fasham et al., 1990; Huisman and Weissing, 1995), in reality, the plankton system is rarely mixed sufficiently well. In marine ecosystems, a strongly heterogeneous, 'patchy' distribution of plankton is widely observed (Fasham, 1978; Martin, 2003; Steele, 1978). Thus, although the nonspatial analysis is useful to provide an early insight into the plankton-oxygen dynamics, an extension of our approach to include explicit space is needed in order to make it more realistic.

There can be different ways to include space into the model. Here we use the "turbulent diffusion" approach where the spatial mixing and the corresponding fluxes of matter are essentially attributed to turbulence and are described by the standard diffusion terms (Monin and Yaglom, 1971). The spatiotemporal dynamics of a plankton system is then described by a system of diffusion-reaction equations where 'reaction' accounts for the (local) population dynamics such as reproduction, mortality, predation etc. Correspondingly, system (11)–(13) takes the following form:

$$\frac{\partial c}{\partial t} = D_T \frac{\partial^2 c}{\partial x^2} + \frac{Au}{c+1} - \frac{\delta u c}{c+c_2} - \frac{\nu c v}{c+c_3} - c, \tag{21}$$

$$\frac{\partial u}{\partial t} = D_T \frac{\partial^2 u}{\partial x^2} + \left(\frac{Bc}{c+c_1} - u\right)u - \frac{uv}{u+h} - \sigma u, \tag{22}$$

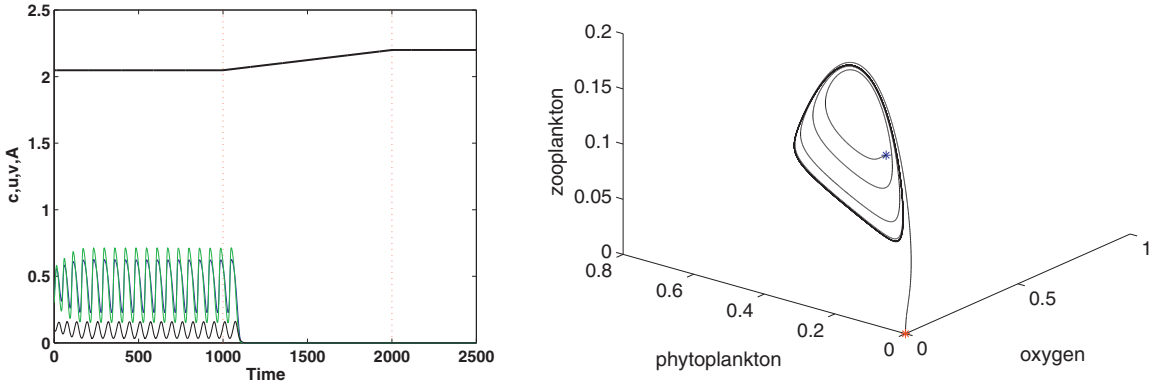

(a) (b)

Fig. 11. (a) Oxygen concentration (blue) and phytoplankton and zooplankton densities (green and black, respectively) against time obtained for $A_0 = 2.048$ and $A_1 = 2.2$. Other parameters and the initial conditions are the same as in Fig. 8. The thick black line at the top shows $A(t)$. (b) Corresponding system trajectory in the phase space of the system. The blue star shows the initial conditions, the red star shows the system state at the end of the simulation run. (For interpretation of the references to colour in this figure legend, the reader is referred to the web version of this article.)

$$\frac{\partial v}{\partial t} = D_T \frac{\partial^2 v}{\partial x^2} + \frac{\eta c^2}{c^2 + c_4^2} \frac{uv}{u+h} - \mu v, \tag{23}$$

where D_T is the coefficient of lateral turbulent diffusion and x is the lateral (horizontal) coordinate. The concentration of dissolved oxygen and plankton densities are now functions of space and time, so that $c = c(x,t)$, $u = u(x,t)$ and $v = v(x,t)$.

Note that, although a more realistic model should consider the plankton-oxygen dynamics in a 2D or 3D space, for sake of simplicity here we only consider its 1D reduction. In terms of a real marine ecosystem, the solution of system (21)–(23) can be interpreted as a transect along the ocean surface. Therefore, the system (21)–(23) apparently does not take into account possible heterogeneity of the plankton vertical distribution. However, we mention here that the phytoplankton density at the ocean surface is known to be a proxy for the column-integrated phytoplankton biomass (Uitz et al., 2006). Moreover, the main controlling factor for the rate of photosynthesis is the sunlight; the sunlight intensity is known to decay with depth very fast, decreasing by an order of magnitude over the 'photic' subsurface layer of about twenty meters (Calbet, 2015). Meanwhile, the vertical distribution of phytoplankton over the top 20–30 meters of the water column is often approximately uniform in open-sea ecosystems, e.g. see Calbet (2015); Cullen (1982); in particular, the deep chlorophyll maximum does not normally occur until 50–100 meters.[4]

We mention that the system (21)–(23) does not take into account the effect of zooplankton self-movement. This is justified by the observation that the intensity of horizontal (lateral) mixing due to zooplankton mobility is several order of magnitude less than the mixing due to marine turbulence and arguably can be neglected (Pinel-Alloul, 1995).

In order to keep in line with our choice of dimensionless variables, see the end of Section 2, we now change x to the dimensionless coordinate $x' = x\sqrt{m/D_T}$. As a result, in the dimensionless system $D_T = 1$; we emphasize that this is not a particular choice of the turbulent diffusion coefficient but just a technical consequence of the change of variables.

It does not seem possible to perform any instructive analytical investigation of the system (21)–(23), we only mention here that the steady states of its nonspatial counterpart (11)–(13) correspond to the spatially uniform steady states of the system (21)–(23). In order to reveal the properties of the spatiotemporal plankton-oxygen dynamics, in particular, its response to the change in the oxygen production rate due to the global warming, Eqs. (21)–(23) are solved numerically in a finite domain $0 < x < L$ (where L is thus the domain length) by finite differences using the zero-flux conditions at the domain boundaries. The mesh steps are chosen as $\Delta x = 0.5$ and $\Delta t = 0.01$. In order to avoid numerical artifacts, it was checked that a decrease in the mesh step size does not lead to any significant change in the numerical results.

Since we are mostly interested in the effect of the climate change on the system dynamics, it is reasonable to assume that, prior to any changes in the oxygen production rate, the system is in a sustainable state or sustainable dynamical regime, i.e. the coexistence state E_3 is either stable or unstable but surrounded by a stable limit cycle. However, the case of E_3 being stable results in a somewhat trivial dynamics where the initial condition would normally converge to the corresponding uniform spatial distribution[5] $c(x,t) \equiv \bar{c}$, $u(x,t) \equiv \bar{u}$ and $v(x,t) \equiv \bar{v}$ where $\bar{c}$, $\bar{u}$ and $\bar{v}$ are the steady state values of the nonspatial system; see Section 3. The system then becomes effectively nonspatial and its response to an increase in A agrees very well with the results shown in Section 4. The case of the existence of a stable limit cycle is much more interesting and possibly more realistic as predator-prey-type oscillations are often observed in nature (Turchin, 2003). For a diffusion-reaction system with oscillatory local dynamics, it is well known (e.g. see Malchow et al. (2008); Medvinsky et al. (2002); Petrovskii and Malchow (2001)) that almost any initial condition results in the onset of spatiotemporal chaos: a spatially irregular dynamical pattern with population densities at any position in space exhibiting complicated irregular oscillations in time.

In order to perform numerical simulations in the system (21)–(23), we consider the following "nearly uniform" initial species

[4] The situation can different in shelf ecosystems and lakes, e.g. see Fig. 1 in Mellard et al. (2011).

[5] For some initial conditions, there may exist travelling fronts connecting the two stable steady states E_0 and E_3; however, since the biological meaning of such 'waves of oxygen' remains obscure, we do not discuss them here for sake of brevity.

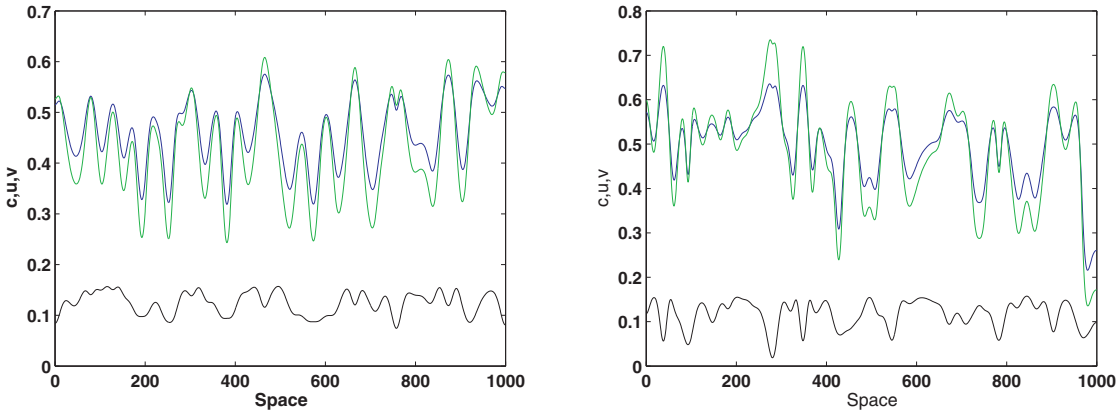

Fig. 12. Distribution of oxygen (blue), phytoplankton (green) and zooplankton (black) over space obtained at $t = 10000$ for $A_0 = 2$ and (a) $A_1 = 2.05$ and (b) $A_1 = 2.06$. Other parameters are given in the text. (For interpretation of the references to colour in this figure legend, the reader is referred to the web version of this article.)

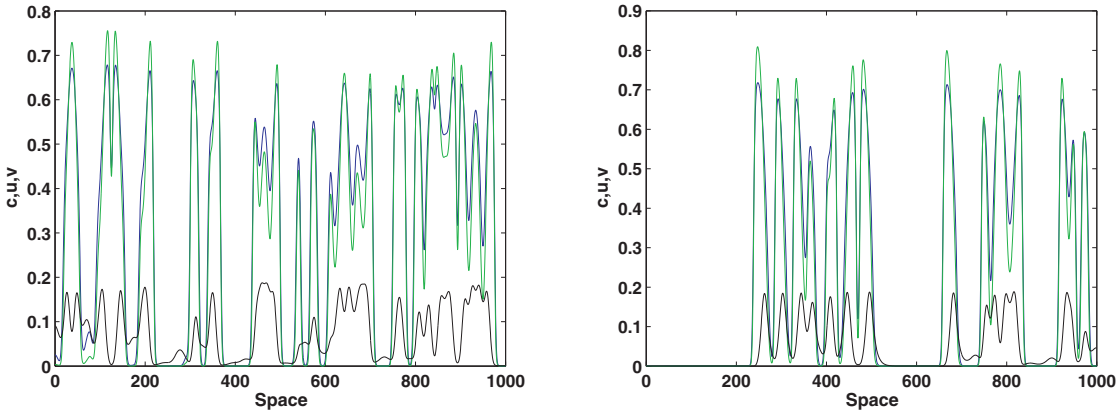

Fig. 13. Distribution of oxygen (blue), phytoplankton (green) and zooplankton (black) over space obtained at $t = 10000$ for $A_0 = 2.05$ and (a) $A_1 = 2.2$ and (b) $A_1 = 2.25$. Other parameters are the same as in Fig. 12. (For interpretation of the references to colour in this figure legend, the reader is referred to the web version of this article.)

distribution:

$$c(x,0) = \bar{c}, \quad u(x,0) = \bar{u}, \quad v(x,0) = \left(x - \frac{L}{2}\right)\frac{\epsilon}{L} + \bar{v}, \tag{24}$$

where ϵ is an auxiliary parameter taken to be small, $\epsilon \ll 1$. However, initial conditions (24) result in a long transient dynamics before the system's inherent state of spatiotemporal chaos is reached (Petrovskii and Malchow, 2001). The interplay between these long transients and the effect of the global warming as given by the dependence of A on time, cf. Eq. (19), may result in a biased prediction about the system properties. Correspondingly, before the effect of warming is modeled, we run the system up to $t = 12000$ to make sure that the transients die out. The time is then reset to zero to correspond to the time in Eq. (19). In the simulation results shown below, "time" therefore refers to the reset time, i.e. where the first period of twelve thousands time units is omitted.

Figs. 12 and 13 show the results obtained for various values of A_0 and A_1, other parameters being fixed as $B = 1.8$, $c_1 = 0.7$, $c_2 = 1$, $c_3 = 1$, $c_4 = 1$, $\nu = 0.01$, $\eta = 0.7$, $\mu = 0.1$, $h = 0.1$, $\sigma = 0.1$ and $\delta = 1$. In the simulations, we fix the time when the warming starts as $t_1 = 1000$ and the moment when it ends as $t_2 = 2000$. After the warming ends and the oxygen production rate stabilizes at a new value $A(t) = A_1$, the system is run for another period of time T to make sure that the possible transients caused by the change in A dies out. The snapshots of the spatial distribution are shown at $t = 10000$, i.e. for $T = 8000$.

Fig. 12a shows the species distribution over space obtained for $A_1 = 2.05$. In this case, the corresponding nonspatial system possesses a stable limit cycle. Formation of the chaotic spatiotemporal pattern is therefore expected (Malchow et al., 2008). The sustainable dynamics of the spatially explicit system agrees well with that of the nonspatial system.

However, for another value of A_1 the situation changes. Fig. 12b shows the species distribution over space obtained for $A_1 = 2.06$. Although it looks qualitatively similar to that shown in Fig. 12a, there is one important difference: for the same value of A_1, the nonspatial system goes extinct. Indeed, a close inspection of Fig. 3 shows that $A_1 = 2.06$ lies outside of the parameter domain of the sustainable dynamics. We therefore conclude that the spatial system is more resilient to the changes in A compared to the corresponding nonspatial system.

This conclusion is further confirmed by simulations for other, bigger values of A_1. Fig. 13 shows the snapshots of the spatial densities of plankton and oxygen over space obtained at $t = 10000$ for $A_1 = 2.2$ and $A_1 = 2.25$, see (a) and (b) respectively. There is no extinction and the patchy dynamics both of oxygen and plankton is

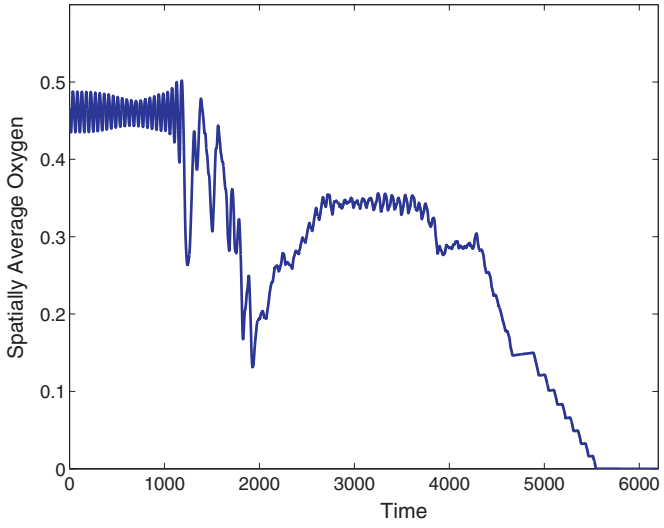

Fig. 14. Spatially average oxygen concentration vs time obtained for $A_0 = 2.05$ and $A_1 = 2.378$, other parameters the same as in Fig. 12.

apparently sustainable in spite of the fact that in both cases the value of A_1 is well outside of the parameter range of sustainable dynamics of the nonspatial system.

The additional resilience of the spatial system has its limits too. When A_1 is sufficiently large ($A \approx 2.3$ or larger for other parameter values fixed as above), the system goes extinct. Fig. 14 shows the spatially average oxygen concentration against time. It is readily seen that the decrease in A first results in irregular oscillations of considerable magnitude combined with a general decrease in the oxygen concentration. Once the oxygen production rate stabilizes at the new value $A = A_1$ at $t = 2000$, the oxygen concentration starts growing with an apparent stabilization at a new value for the period between $t \approx 2700$ and $t \approx 3700$. However, this stabilization is superficial rather than real, so that at a later time the oxygen concentration starts falling again finally resulting in a complete oxygen depletion across the domain.

Interestingly, prior to the extinction the spatial pattern undergoes some subtle changes. We will discuss this issue in detail in the next section.

6. Intermittency, extinction and early warning signals

In order to look more closely into the properties of the species spatial distribution, in particular into the changes caused by a 'sufficiently large' (i.e. that is likely to destabilize the system's dynamics) increase in the oxygen production rate, we perform a series of numerical simulations for fixed values of t_1, t_2 and A_0 and different values of A_1. As well as in the previous section, starting from initial conditions (24) the system is first run up to $t = 12000$ with $A(t) = A_0$ to ensure that it converges to a sustainable dynamical regime (e.g. spatiotemporal chaos). Time is then reset to zero and the system is run for another period of 12,000 time units, now with $A(t)$ given by Eq. (19). Simulations shown below are obtained for $A_0 = 2.05$ (i.e. prior to the warming the nonspatial system is in the regime of stable oscillations, cf. Fig. 8), $t_1 = 100$, $t_2 = 270$ and other parameters having the same values as above.

Snapshots of the oxygen concentration and plankton densities over space obtained at $t = 12000$ are shown in Fig. 15 for two values of A_1. It is readily seen that for a relatively small value of $A_1 = 2.1$, see Fig. 15a, the species spatial distribution after the warming is not much different from that before the warming (cf. Fig. 12) except for it becoming slightly more patchy and the amplitude of the density variation over space increasing. (Note that species persistence at this value of the oxygen production rate is an essentially spatial effect as the nonspatial system is extinct for any $A > 2.06$.) However, the species spatial distribution obtained for a larger value $A_1 = 2.27789$ is drastically different; see Fig. 15b. Instead of the irregular distribution shown in Fig. 15a, now the species densities and oxygen concentration are self-organized into a remarkably regular, almost periodical pattern. The time courses of the spatially average values of the oxygen concentration preceding the distributions of Fig. 15 are shown in Fig. 16a and b, respectively. We observe that the oxygen dynamics corresponding to the nearly periodical spatial distribution is somewhat less stable compared to the irregular one. Variability of the average oxygen concentration differs significantly over time (cf. periods between 2500–3500 and 5500–6500); long periods of small fluctuations around an approximately constant value are punctuated with sudden drops to a much smaller value, e.g. as at $t \approx 4000$.

One question arising here is how the apparent regularity/irregularity seen in the spatial distributions shown in Fig. 15 can be quantified. In order to address this issue, we calculated the corresponding power spectra of the oxygen concentration. The results

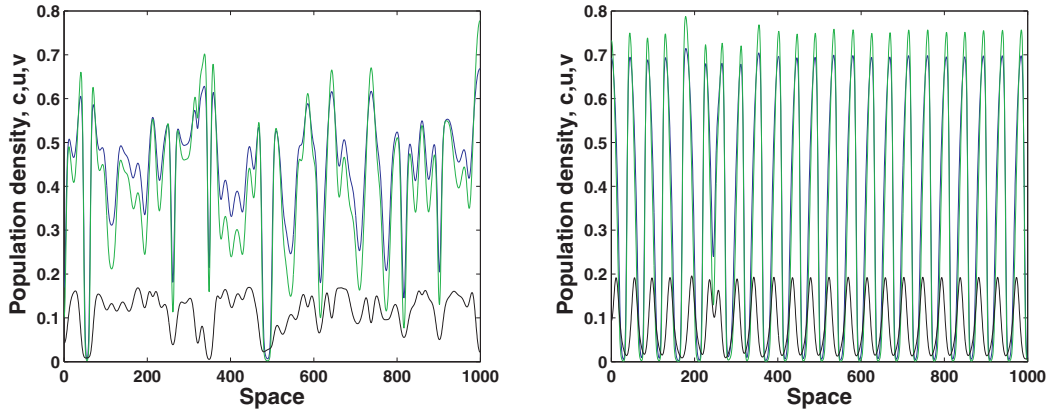

Fig. 15. Snapshots of the oxygen concentration (blue) and the densities of phyto- and zooplankton (green and black, respectively) over space obtained at $t = 12000$ for (a) $A_1 = 2.1$ and (b) $A_1 = 2.27789$. Other parameters are given in the text. (For interpretation of the references to colour in this figure legend, the reader is referred to the web version of this article.)

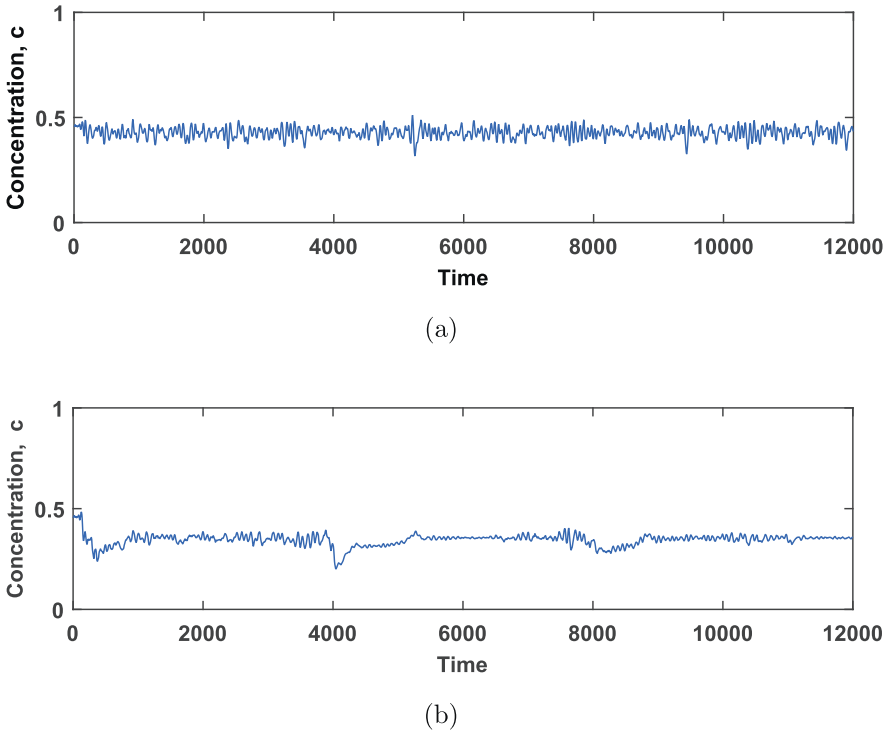

Fig. 16. Spatially averaged concentration of oxygen vs time simulated for the parameters of Fig. 15: (a) for $A_1 = 2.1$, (b) for $A_1 = 2.27789$. Other parameters are given in the text.

are shown in Fig. 17. It is readily seen that, while the power spectrum of the distribution of Fig. 15a does not possess any dominant wavelength, see Fig. 17a, the power spectrum of the pattern shown in Fig. 15b possesses features typical for a periodic pattern such as a sequence of high peaks corresponding to the leading and secondary frequencies (Fig. 17b). Also note that the maximum of the peak at the leading frequency in the power spectrum in Fig. 17b is about fifteen orders of magnitude larger than the maximum of the power spectrum in Fig. 17a. The visual impression of periodicity is therefore confirmed by a quantitative analysis.

A value of A_1 slightly larger than that used in Fig. 15b, namely $A_1 = 2.277895$, results in species extinction and oxygen depletion (not shown here). This is intuitively expected as an increase in A_1 takes the system further away from the parameter range of sustainable dynamics of the *nonspatial* system. Interestingly, however, a further increase in A_1 makes the dynamics of the *spatial* system sustainable again. Fig. 18a shows the spatial distribution of plankton and oxygen obtained for $A_1 = 2.277967$. Obviously, up to the given moment $t = 12000$ there is no extinction. The spatial distribution is not as irregular as it was for smaller values of A_1 but the periodicity is lost either. A further increase in A_1 leads again to a nearly periodical spatial distribution of species, see Fig. 18b obtained for $A_1 = 2.283$. A still further increase (e.g. to $A_1 = 2.286$) leads to plankton extinction again.

We therefore observe that the system response to the global warming (as described by the oxygen production rate $A(t)$ given by Eq. (19)) exhibits an intermittent behavior: the values of A_1 corresponding to sustainable dynamics alternate with values corresponding to extinction. In order to make a more regular insight into this issue, we performed a series of simulations varying A_1 with a very small step. Altogether, over four thousand simulations were run. The results are shown in Fig. 19 where the irregular (chaotic) spatial distributions, periodic patterns and extinctions observed for different values of A_1 are shown by green, yellow and red bars, respectively. It is readily seen that for $A_1 \leq 2.275$ the 'final' (i.e. at the end of the simulation run at $t = 12000$) spatial distribution is always irregular. It then becomes regular in a very small range of values of A_1 before the first extinction happens for $A_1 = 2.275188$. With an increase in A_1, this "irregular→ periodic→ extinction" succession of the system dynamics is repeated several times, cf. the middle part of the diagram. When A_1 becomes sufficiently large, the plankton extinction combined with oxygen depletion becomes the only possible outcome; for $A_1 \geq 2.28559$ (see the last red bar at the right-hand side), we did not observe any single case of system's sustainable dynamics. This range of values of A_1 where species persistence does not occur is preceded by a relatively wide range of values where the spatial pattern is nearly periodical; see the group of yellow bars in the right-hand side of Fig. 19. Moreover, it is readily seen that any extinction event shown in the diagram is preceded by the formation of a periodical pattern. It suggests that the change in the spatial pattern from distinctly irregular to nearly periodical can be regarded as an early warning signal of the approaching catastrophe.

Interestingly, when the extinction/depletion happens, it often happens following a somewhat unusual scenario. Fig. 20 shows the spatially average oxygen concentration against time. The spatially average plankton densities (not shown here) exhibit a similar behavior. The irreversible decay in the oxygen concentration starts approximately at $t = 9000$ (being preceded by an increase between 8000–9000). The increase in A from A_0 to A_1 taking place between $t_1 = 100$ and $t_2 = 270$ is followed by an upward trend in the oxygen concentration clearly seen between $500 < t < 1000$. Between $t \approx 1000$ and $t \approx 8000$ the dynamics of the system is apparently sustainable and one could expect it to remain sustainable indefinitely. However, this intuitive expectation is misleading as the dynamics changes dramatically at $t \approx 8000$. The quasi-sustainable dynamical regime observed between $1000 < t < 8000$ is therefore a long term transient and not an asymptotical dynamics of the system. We mention here that, in the intermittency range of parameter

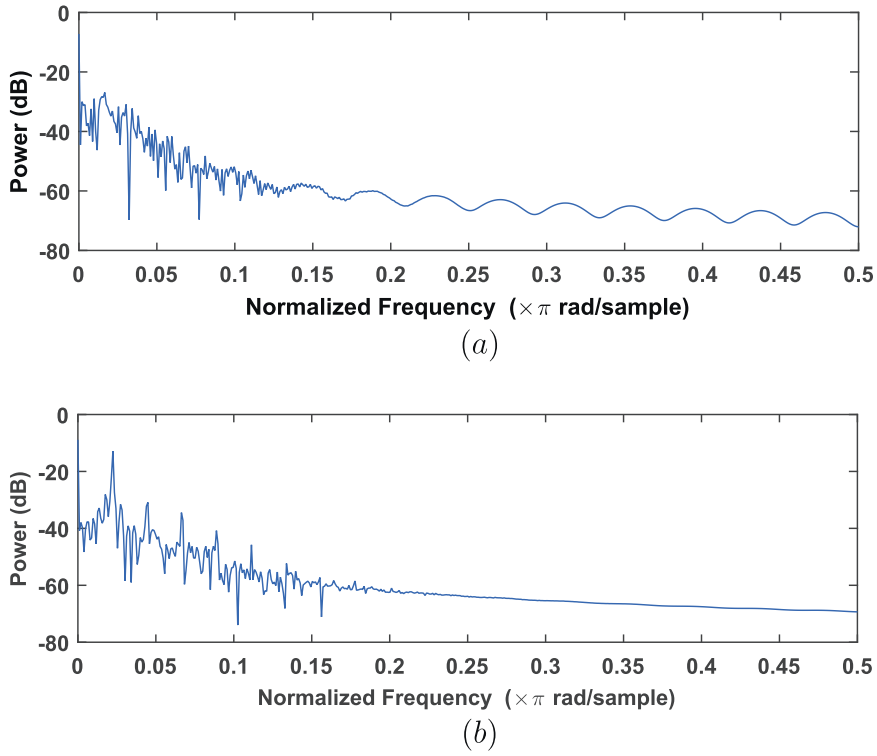

Fig. 17. Power spectra of the spatial distribution of oxygen shown in Fig. 15a and b, respectively.

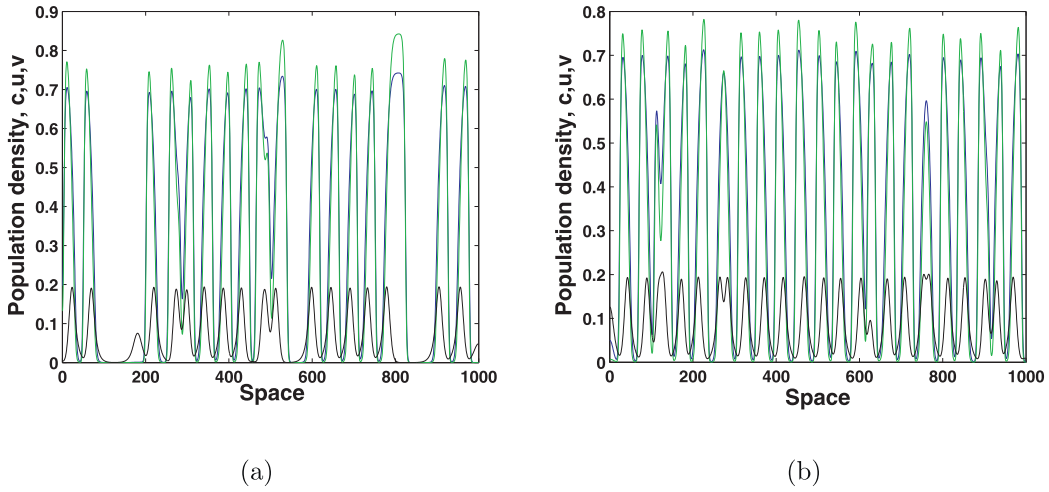

Fig. 18. Snapshots of the oxygen concentration (blue) and the densities of phyto- and zooplankton (green and black, respectively) over space obtained at $t = 12000$ for (a) $A_1 = 2.277967$ and (b) $A_1 = 2.283$. Other parameters are the same as in Fig. 15. (For interpretation of the references to colour in this figure legend, the reader is referred to the web version of this article.)

A_1 (cf. Fig. 19), this scenario of extinction/depletion catastrophe preceded by long-living transient dynamics is typical for the system (21)–(23); most of the extinction events shown in Fig. 19 occur in this manner.

One question remaining is whether the above results are sensitive to the duration of warming τ and to the initial value of the oxygen production rate A_0. In order to address this issue, we performed simulations to determine the value of A_1 at which the intermittent extinction/persistence structure changes to the continuous spectrum of extinction-only values (cf. the right-hand side of Fig. 19) for different τ and A_0 keeping other parameters fixed as above. Fig. 21 shows the results obtained for four different values of A_0 (as shown in the figure legend) and five different values of τ (as shown on the horizontal axis of the figure). We therefore observe that, in the inspected range of parameter values, the critical value of A_1 shows almost no dependence on either τ or A_0. It means that the main factor controlling the system response to the increase in the oxygen production rate A is its final value, i.e. A_1.

7. Discussion and concluding remarks

Dynamics of plankton communities have long been a focus of intense research (Behrenfeld and Falkowski, 1997; Cushing, 1975; Eppley, 1972; Harris, 1986; Hoppe et al., 2002; Steele, 1978). Apart from being the main driver of the ocean primary production, marine phytoplankton is a major producer of oxygen. The amount of

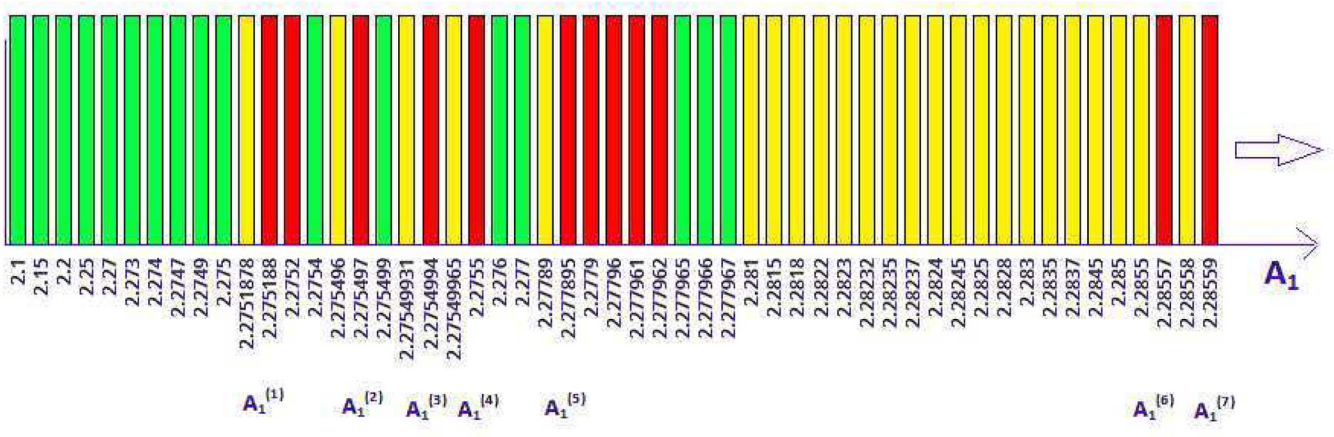

Fig. 19. Fine structure of the plankton-oxygen system response to the final value A_1 of the oxygen production rate $A(t)$ reached in the course of its increase (as given by Eq. (19)). Different colors denotes different outcomes of the dynamics, as observed at $t = 12000$: red for extinction, yellow for persistence with a nearly periodical spatial pattern, green for persistence with an irregular (chaotic) spatial pattern. Parameters are given in the text. (For interpretation of the references to colour in this figure legend, the reader is referred to the web version of this article.)

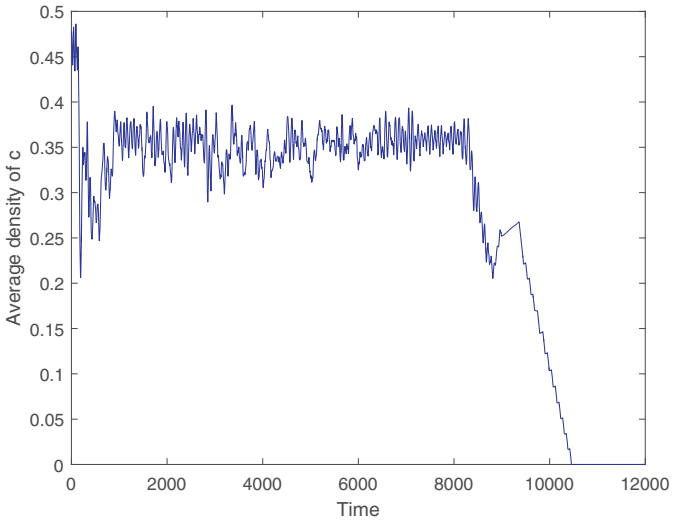

Fig. 20. Spatially average concentration of oxygen vs time simulated for $A_1 = 2.275188$. Other parameters are given in the text.

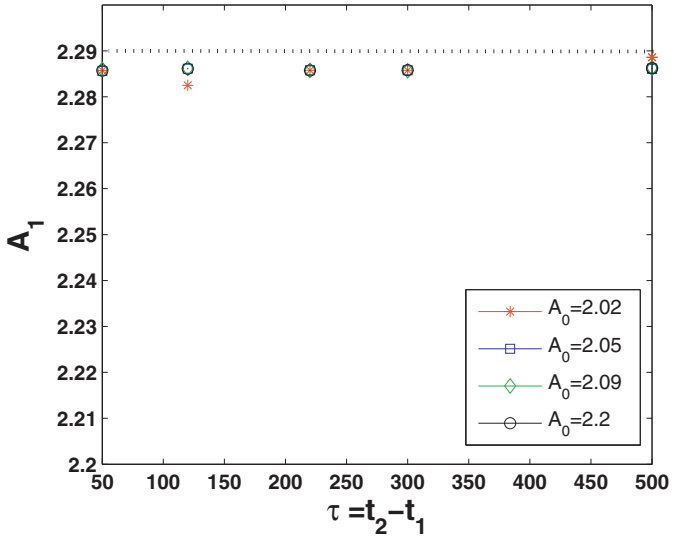

Fig. 21. The critical value of A_1 when extinction becomes the only observed outcome of the system dynamics as a function of τ obtained for four different values of A_0 (shown in the figure legend). The horizontal dotted line is drawn in order to make the visual perception easier.

dissolved oxygen is an important index of the marine ecosystem health (Breitburg et al., 1997; Decker et al., 2004; Canadian Council of Ministers of the Environment, 1999; Krembs, 2012) as anoxic conditions can lead to a mass mortality of the ocean fauna (Diaz and Rosenberg, 2008). Moreover, a considerable part of oxygen produced in the ocean photic layer eventually diffuse to the atmosphere through the ocean surface and contributes to the total stock of the atmospheric oxygen. It is estimated that more than one half of atmospheric oxygen originates in the ocean due to phytoplankton photosynthesis (Harris, 1986; Moss, 2009).

In spite of the evident importance of the marine phytoplankton-oxygen system and, correspondingly, considerable amount of empirical research addressing this issue, it has been largely overlooked by the modelling studies. There is just a handful of papers where the dissolved oxygen is explicitly included into a marine ecosystem model (Allegretto et al., 2005; Dhar and Baghel, 2016; Hull et al., 2000; 2008; Lunardi and DiCola, 2000; Marchettini et al., 1999; Misra, 2010) and none of them consider this issue in the context of the global climate change. In our recent work (Sekerci and Petrovskii, 2015a), we have developed a conceptual model of the coupled plankton-oxygen dynamics and showed that sustainable oxygen production by marine phytoplankton can be severely disrupted by a gradual increase in the average water temperature due to the global warming. Given the scale of the contribution of the phytoplankton-produced oxygen to the oxygen global stock, such a regime shift would likely result in a global oxygen depletion and, consequently, mass mortality of animals and humans. We mention here that regime shifts are observed in many complex ecological systems (Carpenter, 2011; Drake and Griffen, 2010; Lenton, 2008; Litt, 2001; May et al., 2008; McSharry et al., 2003; Scheffer, 2001; Venegas, 2005) and are often followed by species extinction; examples are given by coral reefs (Bellwood et al., 2004), fisheries (Berkes, 2006) and semi-arid vegetation (Kefi, 2007). We showed that this can happen in the plankton-oxygen system too.

In this paper, we report a further progress in understanding the properties of the plankton-oxygen dynamics under climate change. The effect of global warming on plankton dynamics and oxygen production is addressed theoretically by considering a model of a coupled oxygen-phyto-zooplankton dynamics where the rate

of oxygen production by phytoplankton is a function of time to account for the global climate change (see Section 4). The model is described by a system of three coupled ODEs in the nonspatial case and by three corresponding diffusion-reaction PDEs in the spatially explicit case. Biological realism of our model is demonstrated both heuristically and rigourously by showing its relation to a class of more realistic plankton models; see Section 2 and Appendix. The system dynamics in response to the global warming have been studied in detail by means of extensive numerical simulations. We have shown that sustainable dynamics is only possible in a relatively narrow range of parameter values and a sufficiently large change in the oxygen production rate results in a fast plankton extinction and oxygen depletion.

We emphasize that, albeit our model is conceptual and hence relatively simple, it gives an upper bound for a class of more realistic food web type models of marine ecosystem (see Appendix). Therefore, if/when the catastrophe of plankton extinction and oxygen depletion occurs in our model, it necessarily happen in a more complicated model. That indicates a certain generality of our results.

With regard to the bullet-points stated in the introduction, we conclude the following:

- stopping the global warming (e.g., as it is usually presumed, by materially cutting CO2 emission) may not be enough to avert the global ecological disaster as the system can exhibit long term transient behavior. Apparently sustainable dynamics can yet lead to a regime shift after a time lag, with the global oxygen depletion following accordingly. It can therefore be insufficient only to stop the global warming; to prevent the disaster it may be necessary to reverse it to bring the global temperature to its pre-change level. We mention here that long term transient dynamics has been attracting increasing attention recently as it is thought to be a generic mechanism of ecosystems regime shift, extinctions and biodiversity loss (Hastings, 2004; Morozov et al., 2016; Schreiber, 2003; Tilman et al., 1994);
- such a regime shift is not necessarily preceded by any significant drop in the amount of available oxygen, e.g. see the middle part of Fig. 20. However, we observe that there can be other early warning signals of the approaching catastrophe such as a decrease in the temporal variability of the average oxygen concentration (e.g. see Fig. 16) and an increase in the regularity of the species spatial distribution. The latter is known to be an early warning signal of the regime shift in some terrestrial ecosystems (Rietkerk et al., 2004; Kefi et al., 2014).

Note that in the above analysis we mostly focused on a special case where an increase in the water temperature only affected the rate of oxygen production but not other features of the plankton dynamics. This is of course only a caricature of reality as water temperature is known to be a factor controlling also the phytoplankton growth rate (Eppley, 1972; Hoppe et al., 2002). However, once the parameter range of the sustainable dynamics is established, e.g. see Fig. 3, it is straightforward to extend our results onto a more realistic case where the water warming affects both the oxygen production rate A and the phytoplankton growth rate B. Fig. 22 shows a sketch of the corresponding (A, B) parameter plane of the plankton-oxygen system, solid curve for the nonspatial model (11)–(13), dotted curve for its spatial extention (21)–(23). As above, we assume that the plankton-oxygen system is currently in a safe state, so that the corresponding point (shown by a large black dot) lies inside the tongue-shaped domain of sustainable dynamics. Since the maximum rate of phytoplankton cell division tends to increase with temperature (Addy and Green, 1997), the phytoplankton growth rate can be expected to increase too (at least, until the temperature becomes too high). However, in order to attain generality, we consider four possible combinations of various responses of A and B to an increase in the water temperature: both increase (direction North-East), both decrease (direction South-West), A increases and B decreases (direction South-East), A decreases and B increases (direction North-West). In Fig. 22, the corresponding movement of the system through the parameter plane is shown schematically by the arrows. Catastrophe of oxygen depletion happens when the system's path in the parameter plane crosses the boundary of the domain. It is readily seen that the only safe case is the one shown by the green arrow where, in response to an increase in water temperature, the oxygen production rate A decreases and the phytoplankton growth rate B increases. In this case, the change in parameters A and B is likely to keep the system inside the safe range. The opposite case (shown by the orange arrow) where A increases and B decreases is relatively safe if the initial position of the system is far away from the tip of the tongue and unsafe if it is close to the tip. The other two cases shown by red arrows inevitably result (unless the increase in temperature is insignificant) in a regime shift and, consequently, oxygen depletion and a global ecological disaster.

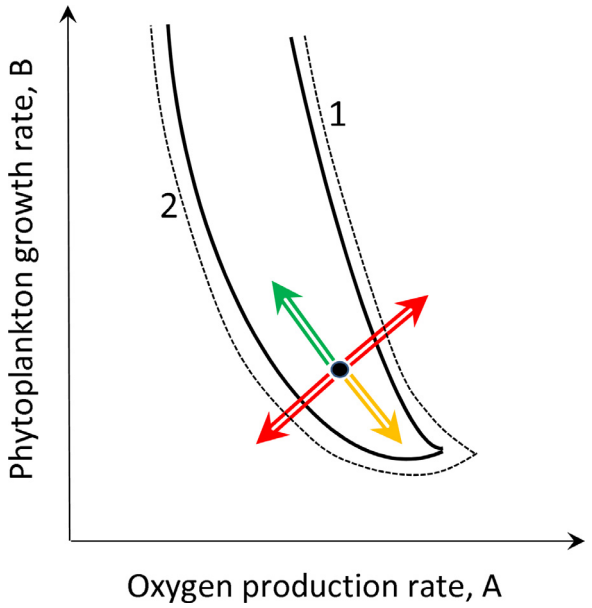

Fig. 22. Sketch of different possible scenarios of the plankton-oxygen system response to global warming. The tongue-shaped domain is the parameter range of sustainable dynamics, solid curves correspond to the nonspatial system, dotted curves take into account the additional resilience of the spatial system. Green and red arrows indicate safe and unsafe scenarios, respectively; orange arrow can be either safe or unsafe; more details in the text. (For interpretation of the references to colour in this figure legend, the reader is referred to the web version of this article.)

We mention here that the regime shift happens differently depending on what part of the domain boundary (denoted in Fig. 22 as curves 1 and 2) is crossed by the system's path as the extinction/deletion is preceded by a different succession of bifurcations. When moving North-East (both A and B increase) and thence crossing Boundary 1, the extinction/depletion is preceded by the onset of spatiotemporal oscillations of an increasing amplitude, cf. the change in the dynamics seen in Fig. 4d → e → f. One might call it Catastrophe Type 1. In the case of moving South-West (both A and B decrease) and thence crossing Boundary 2, the extinction/depletion Catastrophe Type 2 occurs which is not preceded by oscillations, cf. Fig. 4d → c → b → a.

Our study leaves a number of open questions. Firstly, the water temperature is known to affect the oxygen solubility. The maximum possible concentration of dissolved oxygen decreases with an increase in water temperature (Hein et al., 2014; Matear et al., 2000) and it is not immediately clear how this may affect the

rate of oxygen production. Secondly, in our model none of the parameters depend on space, which means that the environment is assumed to be homogeneous. Thus we have disregarded a possible effect of environmental gradients. Although our preliminary insight into this issue (not shown here) did not reveal any significant difference compared to the dynamics of the homogeneous system, this deserves a closer attention. Thirdly, our model does not give any account of possible adaptation of plankton species to the changing environmental conditions, i.e. to the gradual increase in the average water temperature. In principle, there may exist an evolutionary strategy that could keep the system within the safe parameter range and hence prevent the catastrophic regime shift. These issues will become a focus of future research.

Appendix A. Comparison theorem for plankton models

Consider a class of the so called NPZ models of plankton dynamics that can be written in a general form as the following system (Franks, 2002):

$$\frac{dN}{dt} = -\phi(I)\psi(N)P + (1-\kappa_0)e(P,Z) + i(P)P + j_0(Z)Z, \tag{25}$$

$$\frac{dP}{dt} = \phi(I)\psi(N)P - e(P,Z) - i(P)P, \tag{26}$$

$$\frac{dZ}{dt} = \kappa_0 e(P,Z) - j_0(Z)Z, \tag{27}$$

where N, P and Z are, respectively, the densities of nutrients, phytoplankton and zooplankton at time t. Model (25)–(27) takes into account the dependence of phytoplankton growth on the intensity of sunlight I and the availability of nutrients, which is described by functions $\phi(I)$ and $\psi(N)$ respectively. Functions $i(P)$ and $j_0(Z)$ take into account the possible density dependence of the mortality rate of phyto- and zooplankton, respectively, e.g. due to the intra-group or intra-specific competition; $i(P) = Const$ and $j_0(Z) = Const$ if mortality is density independent. Function $e(P, Z)$ describes zooplankton grazing on phytoplankton and κ_0 is the food utilization efficiency. The presence of the terms $i(P)P$ and $j_0(Z)Z$ in Eq. (25) accounts for detritus recycling; for more details see Franks (2002).

NPZ models have been extensively used in marine ecology either by themselves or as building blocks of more complicated models. Indeed, one can make the model (25)–(27) more realistic by including higher trophic levels, e.g. to account planktivorous fish, predatory fish, sharks etc. NPZ model then turns into a food chain or food web model. Since out focus is on the dynamics of oxygen and the rate of its production/consumption, we also include the dissolved oxygen c and take into account that availability of oxygen is likely to be a controlling factor for several processes involved. In particular, there is biological evidence that dissolved oxygen can be a factor controlling phytoplankton growth (Franke et al., 1999), especially under anoxic conditions. Model (25)–(27) then takes the following form:

$$\frac{dc}{dt} = A(I)f(c)P - u_r(c,P) - v_r(c,Z) - \sum_{k=1}^{n} f_{r,k}(c,F_k) - mc, \tag{28}$$

$$\frac{dN}{dt} = -\phi(I)\psi(c,N)P + (1-\kappa_0)e(P,Z) + i(P)P + j_0(Z)Z + \sum_{k=1}^{n} j_k(F_k)F_k, \tag{29}$$

$$\frac{dP}{dt} = (\phi(I)\psi(c,N) - i(P))P - e(P,Z) - \sum_{k=1}^{n} d_k(P)F_k, \tag{30}$$

$$\frac{dZ}{dt} = \kappa_0 e(P,Z) - j_0(Z)Z - \sum_{k=1}^{n} r_k(Z)F_k, \tag{31}$$

$$\frac{dF_1}{dt} = \kappa_{1,P}(c)d_1(P)F_1 + \kappa_{1,Z}r_1(Z)F_1 - j_1(F_1)F_1 - \sum_{k=2}^{n} q_k(F_1)F_k, \tag{32}$$

$$\cdots$$

$$\frac{dF_n}{dt} = \left[\sum_{k=1}^{n-1} \kappa_{n,k}(c)q_k(F_k)\right]F_n - j_n(F_n)F_n, \tag{33}$$

cf. (Franks, 2009; Prowe et al., 2012). Here F_k is the population density of animals (e.g. fish species) at the kth trophic level at time t, $k = 1, \ldots, n$. Functions d_k and r_k describe the density-dependent efficiency of predation of, respectively, phyto- and zooplankton by the species at the kth trophic level, coefficients q_k describe the predation pressure on the kth level from higher predators, κ_k is the food utilization efficiency at the kth tropic level. All coefficients are nonnegative; some of them can be zero to account for biological traits and/or food preference. For instance, large fish like tuna (which constitutes the $(n-1)$th level of the food chain) is unlikely to feed on phytoplankton, hence $d_{n-1}(P) \equiv 0$. Note that model (28)–(33) describes a food web rather than a food chain, because it takes into account intra-guild predation.

System (28)–(33) is apparently very complicated. However, in case the focus is on its plankton-oxygen subsystem, it can be greatly simplified, importantly, without loosing the mathematical rigor. More specifically, we note that, by omitting certain terms in the right-hand side, we can construct an *upper bound*. Consider, for instance, Eq. (28):

$$\begin{aligned}\frac{dc}{dt} &= A(I)f(c)P - u_r(c,P) - v_r(c,Z) - \sum_{k=1}^{n} f_{r,k}(c,F_k) - mc \\ &\le A(I)f(c)P - u_r(c,P) - v_r(c,Z) - mc \\ &\le \bar{A}f(c)P - u_r(c,P) - v_r(c,Z) - mc,\end{aligned} \tag{34}$$

where we additionally took into account that, since for biological reasons $A(I)$ is obviously a bounded function, there exists $\bar{A}$ such as $A(I) \le \bar{A}$ for any light intensity I.

Similarly, for Eq. (27) we obtain:

$$\frac{dZ}{dt} = \kappa_0 e(P,Z) - j_0(Z)Z - \sum_{k=1}^{n} r_k(Z)F_k \le \kappa_0 e(P,Z) - j_0(Z)Z. \tag{35}$$

In the equation for the phytoplankton growth, we additionally take into account that, for biological reasons function ψ is bounded from above; therefore, there exists $\bar{\psi}(c)$ such as $\psi(c,N) \le \bar{\psi}(c)$ for any N and c. For instance, as $\psi(N)$ is usually a monotonously increasing function (Franks, 2002), one can take $\bar{\psi}(c) = \lim_{N\to\infty} \psi(c,N)$. Also, similarly to the above, $\phi(I)$ is a bounded function, so that there is $\bar{\phi}$ such as $\phi(I) \le \bar{\phi}$ for any I. For Eq. (30), we then obtain:

$$\begin{aligned}\frac{dP}{dt} &= \phi(I)\psi(c,N)P - e(P,Z) - i(P)P - \sum_{k=1}^{n} d_k(P)F_k \\ &\le \phi(I)\psi(c,N)P - e(P,Z) - i(P)P \\ &\le \bar{\phi}\bar{\psi}(c)P - e(P,Z) - i(P)P.\end{aligned} \tag{36}$$

We notice that, as a result, the dependence of nutrient concentration has disappeared from the right-hand side of (36).

Let us now consider the system (28)–(33) where the right-hand side of Eqs. (28), (30) and (31) is changed to their respective upper

bound as given by inequalities (34)–(36):

$$\frac{dc}{dt} = \bar{A}f(c)P - u_r(c,P) - v_r(c,Z) - mc, \tag{37}$$

$$\frac{dN}{dt} = -\phi(I)\psi(c,N)P + (1-\kappa)e(P,Z) + i(P)P + j_0(Z)Z + \sum_{k=1}^{n} j_k(F_k)F_k, \tag{38}$$

$$\frac{dP}{dt} = (\bar{\phi}\bar{\psi}(c) - i(P))P - e(P,Z), \tag{39}$$

$$\frac{dZ}{dt} = \kappa_0 e(P,Z) - j_0(Z)Z, \tag{40}$$

$$\frac{dF_1}{dt} = \kappa_{1,P}(c)d_1(P)F_1 + \kappa_{1,Z}r_1(P)F_1 - j_1(F_1)F_1 - \sum_{k=2}^{n} q_k(F_1)F_k, \tag{41}$$

$$\cdots$$

$$\frac{dF_n}{dt} = \left[\sum_{k=1}^{n-1} \kappa_{n,k}(c)q_k(F_k)\right]F_n - j_n(F_n)F_n. \tag{42}$$

System (37)–(42) does not necessarily possess an immediate biological meaning as such, because the balance of the mass flows is now broken. However, it appears to be an important mathematical tool to provide information about the biologically meaningful system (28)–(33). Namely, by virtue of the *comparison principle* for ordinary differential equations, e.g. see Halil (2002), the solution of system (37)–(42) is an upper bound for the solution of the original system (28)–(33). In particular, if the plankton as described by the model (37)–(42) goes extinct and/or oxygen gets depleted, it means that the extinction/depletion will necessarily happen in the model (28)–(33).

Next, we note that Eqs. (37), (39) and (40) split off the system (37)–(42), because they do not contain variables $F_1, \ldots, F_n$ and N, and hence the sub-system consisting of Eqs. (37), (39) and (40) can be studied independently of the rest of system (37)–(42).

Finally, we observe that this sub-system effectively coincide with our system (2)–(4) (subject to the obvious change of notations). Therefore, we conclude that, by virtue of the *comparison principle* the solution of the system (2–4) provides an upper bound for the plankton density and oxygen concentration given by the system (28)–(33). Whenever species extinction/oxygen depletion happens in system (2)–(4), it necessarily happen in system (28)–(33).

In conclusion, we mention that the system (28)–(33) is not the only case where the conceptual system (2)–(4) works as the upper bound. One could readily think about its extensions (for instance to include different types of nutrients) that would still be bounded by system (2)–(4). Even more importantly, we mention that the spatially explicit system (21)–(23) works as an upper bound for the corresponding spatial extension of the system (28)–(33) to include the turbulent diffusion. By virtue of the comparison principle (theorem) for nonlinear PDEs (Protter and Weinberger, 1984; Volpert and Khudyaev, 1985), the solution of system (21)–(23) gives an upper bound for the solution of the spatial extention of system (28)–(33) and plankton extinction/oxygen depletion in the system (21)–(23) necessarily means the extinction/depletion in the spatial food web model.

References

Addy, K., Green, L., 1997. Dissolved oxygen and temperature. Natural Resources. Fact Sheet No.96-3

Allegretto, W., Mocenni, C., Vicino, A., 2005. Periodic solutions in modelling lagoon ecological interactions. J. Math. Biol. 51, 367–388.

Allgower, E.L., Georg, K., 2003. Introduction to numerical continuation methods, 45. SIAM Classics in Applied Mathematics.

Andersson, A., Haecky, P., Hagström, A., 1994. Effect of temperature and light on the growth of micro-nano-and pico-plankton: impact on algal succession. Mar. Biol. 120 (4), 511–520.

Banse, K., 1995. Zooplankton: pivotal role in the control of ocean production I. Biomass and production. ICES J. Mar. Sci. 52, 265–277.

Behrenfeld, M.J., Falkowski, P.G., 1997. A consumers guide to phytoplankton primary productivity models. Limnol. Oceanogr 42, 1479–1491.

Bellwood, D.R., Hughes, T.P., Folke, C., Nystram, M., 2004. Confronting the coral reef crisis. Nature 429, 827–833.

Berkes, F., et al., 2006. Globalization, roving bandits, and marine resources. Science 311, 1557–1558.

Breitburg, D.L., Loher, T., Pacey, C.A., Gerstein, A., 1997. Varying effects of low dissolved oxygen on trophic interactions in an estuarine food web. Ecol. Monogr 67, 489–507.

Calbet, A., et al., 2015. Heterogeneous distribution of plankton within the mixed layer and its implications for bloom formation in tropical seas. Sci. Rep. 5, 11240.

Canadian Council of Ministers of the Environment, 1999. Canadian Water Quality Guidelines for the Protection of Aquatic Life - Dissolved Oxygen (Marine). Winnipeg, Manitoba.

Carpenter, S.R., et al., 2011. Early warnings of regime shifts: a whole-ecosystem experiment. Science 332 (6033), 1079–1082.

Chapelle, A., et al., 2000. Modelling nitrogen, primary production and oxygen in a Mediterranean lagoon. Impact of oysters farming and inputs from the watershed 127 (2), 161–181.

Childress, J.J., 1976. Effects of pressure, temperature and oxygen on the oxygen consumption rate of the midwater copepod Gaussia princeps. Mar. Biol. 39 (1), 19–24.

Cullen, J.J., 1982. The deep chlorophyll maximum: comparing vertical profiles of chlorophyll α. Can. J. Fish. Aquat.Sci. 39 (5), 791–803.

Cushing, D.H., 1975. Marine Ecology and Fisheries. Cambridge University Press, Cambridge.

Decker, M.B., Breitburg, D.L., Purcell, J.E., 2004. Effects of low dissolved oxygen on zooplankton predation by the ctenophore Mnemiopsis Leidyi. Mar. Ecol. Prog. Ser. 280, 163–172.

Denaro, G., et al., 2013. Dynamics of two picophytoplankton groups in Mediterranean sea: analysis and prediction of the deep chlorophyll maximum by a stochastic reaction-diffusion-taxis model. PLoS ONE 8, e66765.

Dhar, J., Baghel, R.S., 2016. Role of dissolved oxygen on the plankton dynamics in spatio-temporal domain. Model. Earth Syst. Environ. 2, 6.

Diaz, R.J., Rosenberg, R., 2008. Spreading dead zones and consequences for marine ecosystems. Science 321, 926–929.

Drake, J.M., Griffen, B., 2010. Early warning signals of extinction in deteriorating environments. Nature 467 (7314), 456–459.

Eppley, R.W., 1972. Temperature and phytoplankton growth in the sea. Fishery Bull. 70 (4), 1063–1085.

Fasham, M., 1978. The statistical and mathematical analysis of plankton patchiness. Oceanogr. Mar. Biol.: Ann. Rev. 16, 43–79.

Fasham, M.J.R, Ducklow, H.W., McKelvie, S.M., 1990. A nitrogen-based model of plankton dynamics in the oceanic mixed layer. J. Mar. Res. 48, 591–639.

Franke, U., Hutter, K., Johnk, K., 1999. A physical-biological coupled model for algal dynamics in lakes. Bull. Math. Biol. 61, 239–272.

Franks, PJS., 2009. Planktonic ecosystem models: perplexing parameterizations and a failure to fail. J. Plankton Res. 31, 1299–1306.

Franks, P.J.S., 2002. NPZ models of plankton dynamics: their construction, coupling to physics, and applications. J. Oceanogr. 58, 379–387.

Halil, H., 2002. Nonlinear Systems, 3rd New Jersey: Prentice Hall.

Hancke, K., Glud, R.N., 2004. Temperature effects on respiration and photosynthesis in three diatom-dominated benthic communities. Aquat. Microb. Ecol. 37, 265–281.

Hansen, J., Ruedy, R., Sato, M., Lo, K., 2010. Global surface temperature change. Rev. Geophys. 48, RG4004.

Hansen, J., Ruedy, R., Sato, M., Lo, K., Lea, D.W., Medina-Elizade, M., 2006. Global temperature change. PNAS 103, 14288–14293.

Harris, G.P., 1986. Phytoplankton Ecology: Structure, Function and Fluctuation. Springer, Berlin.

Hastings, A., 2004. Transients: the key to long-term ecological understanding? Trends Eco. Evol. 19, 39–45.

Hein, B., Viergutz, C., Wyrwa, J., Kirchesch, V., Schöl, A., 2014. Modelling the impact of climate change on phytoplankton dynamics and the oxygen budget of the Elbe river and estuary (Germany). ICHE 2014. Hamburg-Lehfeldt and Kopmann (eds), pp. 1035–1042.

Hoppe, H.-G., Gocke, K., Koppe, R., Begler, C., 2002. Bacterial growth and primary production along a North–South transect of the Atlantic Ocean. Nature 416 (6877), 168–171.

Huisman, J., Weissing, F.J., 1995. Competition for nutrients and light in a mixed water column: a theoretical analysis. Am. Nat. 146, 536–564.

Hull, V., Mocenni, C., Falcucci, M., Marchettini, N., 2000. A trophodynamic model for the lagoon of Fogliano (Italy) with ecological dependent modifying parameters. Ecol. Modell. 134, 153–167.

Hull, V., Parrella, L., Falcucci, M., 2008. Modelling dissolved oxygen dynamics in coastal lagoons. Ecol. Modell 211, 468–480.

Intergovernmental Panel on Climate Change, 2014. Climate change 2014: synthesis report. Contribution of Working Groups I., II and III to the Fifth Assessment Report of the Intergovernmental Panel on climate change (Core Writing Team). IPCC, Geneva.
Jones, R., 1977. The importance of temperature conditioning to the respiration of natural phytoplankton communities. Br. Phycological J. 12 (3), 277–285.
Kefi, S., et al., 2007. Spatial vegetation patterns and imminent desertification in Mediterranean arid ecosystems. Nature 449, 213–217.
Kefi, S., Guttal, V., Brock, W.A., Carpenter, S.R., Ellison, A.M., Livina, V.N., Seekell, D.A., Scheffer, M., van Nes, E.H., Dakos, V., 2014. Early warning signals of ecological transitions: methods for spatial patterns. PLoS ONE 9, e92097.
Krembs, C., 2012. Marine Water Condition Index. Washington State Department of Ecology. Washington State Department of Ecology, Olympia, WA. Publication No. 12-03–013. https://fortress.wa.gov/ecy/publications/summarypages/1203013.html.
Kremer, J., Nixon, S.W., 1978. A Coastal Marine Ecosystem: Simulation and Analysis. Springer, Berlin.
Lenton, T.M., et al., 2008. Tipping elements in the Earth's climate system. Proc. Natl. Acad. Sci., USA 105, 1786–1793.
Li, W., Smith, J., Platt, T., 1984. Temperature response of photosynthetic capacity and carboxylase activity in Arctic marine phytoplankton. Mar. Ecol. Prog. Ser..
Litt, B., et al., 2001. Epileptic seizures may begin hours in advance of clinical onset: a report of five patients. Neuron 30, 51–64.
Lunardi, F., DiCola, G., 2000. Oxygen dynamics in coastal and lagoon ecosystems. Math. Comput. Mod. 31, 135–141.
Malchow, H., Petrovskii, S.V., Hilker, F.M., 2003. Models of spatiotemporal pattern formation in plankton dynamics. Nova Acta Leopold. NF 88, 325–340.
Malchow, H., Petrovskii, S.V., Venturino, E., 2008. Spatiotemporal Patterns in Ecology and Epidemiology: Theory, Models, and Simulation. CRC Press, Boca Raton.
Mann, K.H., Lazier, J.R.N., 1996. Dynamics of Marine Ecosystems: Biological-Physical Interactions in the Oceans. Oxford: Blackwell, p. 394.
Marchettini, N., Mocenni, C., Vicino, A., 1999. Integrating slow and fast dynamics in a shallow water coastal lagoon. Anal. Chim. 89, 505–514.
Martin, A.P., 2003. Phytoplankton patchiness: the role of lateral stirring and mixing. Progr. Oceanogr. 57, 125–174.
Matear, R., Hirst, A., McNeil, B., 2000. Changes in dissolved oxygen in the Southern Ocean with climate change. Geochem. Geophys. Geosyst. 1 (11).
May, R.M., Levin, S.A., Sugihara, G., 2008. Ecology for bankers. Nature 451, 893–895.
McSharry, P.E., Smith, L.A., Tarassenko, L., 2003. Prediction of epileptic seizures: are nonlinear methods relevant? Nat. Med. 9, 241–242.
Medvinsky, A.B., Petrovskii, S.V., Tikhonova, I.A., Malchow, H., Li, B-L, 2002. Spatiotemporal complexity of plankton and fish dynamics. SIAM Rev. 44, 311–370.
Mellard, J.P., Yoshiyama, K., Litchman, E., Klausmeier, C.A., 2011. The vertical distribution of phytoplankton in stratified water columns. J. Theor. Biol. 269, 16–30.
Misra, A., 2010. Modeling the depletion of dissolved oxygen in a lake due to submerged macrophytes. Nonlinear Anal. Modell. Cont 15, 185–198.
Monin, A.S., Yaglom, A.M., 1971. Statistical Fluid Mechanics: Mechanics of Turbulence, 1. MIT Press, Cambridge MA.
Morozov, A.Y., Banerjee, M., Petrovskii, S.V., 2016. Long-term transients and complex dynamics of a stage-structured population with time delay and the Allee effect. J. Theor. Biol. 396, 116–124.
Moss, B.R., 2009. Ecology of Fresh Waters: Man and Medium, Past to Future. John Wiley & Sons, London.
Petrovskii, S., Malchow, H., 2001. Wave of chaos: new mechanism of pattern formation in spatio-temporal population dynamics. Theor. Popul. Biol. 59, 157–174.
Petrovskii, S.V., Malchow, H., 2004. Mathematical models of marine ecosystems. The Encyclopedia of Life Support Systems (EOLSS). EOLSS Publishers, Oxford UK.
Pinel-Alloul, B., 1995. Spatial heterogeneity as a multiscale characteristic of zooplankton community. Hydrobiologia 300/301, 17–42.
Protter, M.H., Weinberger, H.F., 1984. Maximum Principles in Differential Equations. Springer, New York.
Prowe, AEF., Pahlow, M., Dutkiewicz, S., Follows, M., Oschlies, A., 2012. Topdown control of marine phytoplankton diversity in a global ecosystem model. Progr. Oceanogr. 101, 1–13.
Rietkerk, M., Dekker, S.C., de Ruiter, P.C., van de Koppel, J., 2004. Self-organized patchiness and catastrophic shifts in ecosystems. Science 305, 1926–1929.
Robinson, C., 2000. Plankton gross production and respiration in the shallow water hydrothermal systems of Milos,Aegean Sea. J. Plankton Res. 22, 887–906.
Scheffer, M., et al., 2001. Catastrophic shifts in ecosystems. Nature 413, 591–596.
Schreiber, S., 2003. Allee effects, chaotic transients, and unexpected extinctions. Theor. Popul. Biol. 64, 201–209.
Sekerci, Y., Petrovskii, S., 2015a. Mathematical modelling of plankton–oxygen dynamics under the climate change. Bull. Math. Biol. 77 (12), 2325–2353.
Sekerci, Y., Petrovskii, S., 2015b. Mathematical modelling of spatiotemporal dynamics of oxygen in a plankton system. Math. Modell. Nat. Phenom. 10 (2), 96–114.
Steel, J.A., 1980. Phytoplankton models. In: LeCren, E.D., Lowe-McConnell, R.H. (Eds.), Functioning of Freshwater Ecosystems, Vol. 2. Cambridge University Press, Cambridge, pp. 220–227.
Steele, J.H., 1978. Spatial Pattern in Plankton Communities. Springer Science & Business Media.
Tilman, D., May, R.M., Lehman, C.L., Nowak, M.A., 1994. Habitat destruction and the extinction debt. Nature 371, 65–66.
Turchin, P., 2003. Complex Population Dynamics: A Theoretical/Empirical Synthesis. Princeton University Press.
Uitz, J., Claustre, H., Morel, A., Hooker, S.B., 2006. Vertical distribution of phytoplankton communities in open ocean: an assessment based on surface chlorophyll. J. Geophys. Res. 111, C08005.
Valenti, D., et al., 2015. How diffusivity, thermocline and incident light intensity modulate the dynamics of deep chlorophyll maximum in Tyrrhenian sea. PLoS ONE 10, e0115468.
Valenti, D., et al., 2016. Stochastic models for phytoplankton dynamics in Mediterranean sea. Ecol. Complex. 27, 84–103.
Venegas, J.G., et al., 2005. Self-organized patchiness in asthma as a prelude to catastrophic shifts. Nature 434, 777–782.
Volpert, A.I., Khudyaev, S.I., 1985. Analysis in Classes of Discontinuous Functions and Equations of Mathematical Physics. Nijoff, Dordrecht.